The Cryosphere, 20, 7049–7084, 2026
https://doi.org/10.5194/tc-20-7049-2026
© Author(s) 2026. This work is distributed under
the Creative Commons Attribution 4.0 License.

The Cryosphere Open Access EGU

Snowmelt influence on Northern Hemisphere river discharge – the potential of causal inference for assessing long-term trends

Samuel Schilling[1], **Tobias Bolch**[2], **Andreas Dietz**[1], **Rebecca Jean Herman**[3,4], **and Claudia Kuenzer**[1,5]

[1]German Remote Sensing Data Center, German Aerospace Center, DLR, 82234 Weßling, Germany
[2]Institute of Geodesy, Graz University of Technology, Graz, Austria
[3]Center for Scalable Data Analytics and Artificial Intelligence, ScaDS.AI Dresden/Leipzig, 01062 Dresden, Germany
[4]Department of Computer Science, University of Potsdam, Potsdam, Germany
[5]Institute for Geography and Geology, University of Wuerzburg, 97074 Wuerzburg, Germany

Correspondence: Samuel Schilling (samuel.schilling@unibe.ch)

Received: 16 December 2025 – Discussion started: 23 February 2026
Revised: 28 October 2026 – Accepted: 10 November 2026 – Published: 27 November 2026

Abstract. Snowmelt is a vital contributor to river discharge across the Northern Hemisphere, supplying freshwater to over 1.5 billion people and supporting key economic sectors such as agriculture and hydropower. However, climate change has led to a decline in snow water equivalent (SWE) on almost the entire Northern Hemisphere, reducing snow-based water availability. Despite the importance of snowmelt and the pressure imposed by climate change, no large-scale studies have examined the connection between snowmelt dynamics and river discharge beyond statistical measures, which fail to capture the complexity of hydrological regimes. To address this gap, we apply PCMCI+, a method that adapts the PC algorithm proposed by Peter Spirtes and Clark Glymour to the time-series setting. We use it to derive qualitative causal structures across 119 basins from 1980 to 2022 and then quantify the causal effects using a 20-year moving window and a random-forest estimator. Our results show that the role of snowmelt in streamflow generation is changing. In various basins where the method allows for trend detection, the causal effect of snowmelt on river discharge, normalized by mean river discharge, is increasing despite declining SWE. This suggests that the growing causal role of snowmelt is primarily driven by increasing anomalies in snowmelt itself, rather than by a strengthening coupling between snowmelt and discharge, in certain basins despite a generally declining SWE. While regional differences emerge, causal effects do not consistently correlate with geographical factors such as latitude or basin characteristics. Analyses in six basins that serve as illustrative examples indicate that changes in seasonal hydrology, particularly the timing and distribution of precipitation, influence the relative role snowmelt plays for river discharge. These findings demonstrate the potential of causal inference as a complement to conventional statistical measures in the analysis of large-scale snow hydrological regimes.

1 Introduction

1.1 Snow as a river flow driver

In various regions of the world, especially in the Northern Hemisphere, snowmelt is the dominant streamflow driver and serves as the primary freshwater source for over 1.5 billion people worldwide and thus their economic, societal and environmental livelihoods. (Barnett et al., 2005; UN DESA, 2022). Unlike rain, snow not only serves as a water resource but also as a storage mechanism. Snow accumulates mainly during winter and contributes to streamflow during the ablation phase, entering the stream through overland flow, subsurface flow, or intermediate storage such as glaciers and groundwater (DeWalle and Rango, 2008; Viviroli et al., 2007; Tague and Grant, 2009). Downstream, the water is subsequently used for various purposes.

However, the reliability of snow-dominated rivers as a freshwater resource is deteriorating due to changes induced by anthropogenic global warming in the upstream snowpacks (Fig. 1, label 11, Immerzeel et al., 2020; Gottlieb and

Mankin, 2024). The most fundamental change is a decline in snow cover in the Northern Hemisphere. An analysis of various large-scale studies, with over 30 years of temporal coverage, has shown that there is a consensus on a decreasing snow water equivalent (SWE) trend, considering certain regional and seasonal differences (Schilling et al., 2024). This declining trend has various consequences. For instance, a smaller snowpack means reduced snowmelt and seasonality of the streamflow, decreasing the temporal reliability of snow as a freshwater resource (Han et al., 2024; Wang et al., 2024). In addition, higher temperatures, especially in spring, can cause earlier and faster snowmelt, and can further raise flood risk by increasing the occurrence of rain-on-snow events (Fig. 1, label 4, Musselman et al., 2018; Maina and Kumar, 2023).

Downstream, several systems crucial for human livelihood are increasingly subjected to the impacts of these changes, as schematically shown in Fig. 1. Agriculture in snow-dominated regions, for example, is closely tied to the availability of water from snowmelt and can therefore suffer reduced harvests and crop failure (Fig. 1, label 7, Qin et al., 2022; Huning and AghaKouchak, 2020). Other economic sectors such as hydropower (Fig. 1, label 3, Soomro et al., 2024), inland cargo shipping (Fig. 1, label 6, Schweighofer, 2014; Bedoya-Maya et al., 2024), and tourism (Fig. 1, label 1, François et al., 2023), which in some regions are reliant on consistent snowpacks, are also affected. Additionally the changing snowpack intensifies the demand on civil infrastructure regarding heightened flood risk (Fig. 1, label 4, Zhou et al., 2022), or snow avalanches (Fig. 1, label 2, Eckert et al., 2024). Communities, especially indigenous peoples, who are heavily affected by these developments also experience changes in their cultures and languages (Fig. 1, label 10) and are sometimes also forced to migrate to safer places (Fig. 1, label 5, Ford et al., 2021; Reyes-García et al., 2024). Finally, the effects of changing global snow cover extend beyond human systems, influencing flora and fauna through numerous ecological processes (Fig. 1, label 9, Inouye, 2022; Slatyer et al., 2024; Wenzl et al., 2024).

Figure 2 shows the ratio of snowmelt to total precipitation in 119 river basins. This ratio serves as a measure of snow dominance, highlighting regions where and to what extent snow contributes to streamflow generation. Generally the snow dominance increases with latitude, and around major mountain ranges (compare Fig. 2 right insert c). Figure 2b shows the normalized average of total precipitation, as an indication for the general hydroclimatology in the analyzed basins. This provides context for interpreting the snowmelt-to-precipitation ratio, as basins with lower total precipitation tend to show relatively higher ratios.

Despite this extensive research on Northern Hemisphere snow water equivalent (SWE), since 2000, only a minority of large-scale studies have connected SWE to broader contexts in their design or data use (Schilling et al., 2024; Gordon et al., 2022). When such links were made, they focused almost exclusively on water availability, including terrestrial water storage (TWS), river discharge, or droughts, with only few studies extending beyond these topics. There were two studies that linked SWE to TWS on a global scale (Zhang et al., 2019; Tangdamrongsub et al., 2021) and one hemispherical analysis (Girotto et al., 2021). Furthermore Han et al. (2024) connected SWE to streamflow on a hemispheric scale linking snow fraction to streamflow seasonality across 3,049 catchments in the Northern Hemisphere. However, this study addresses the timing rather than the magnitude of snowmelt's contribution to discharge. Other studies conducted beyond a national or basin scale linking river discharge to SWE were two Pan-Arctic studies (Rawlins et al., 2007; Biancamaria et al., 2011), and when the scope is extended to snow cover research, only one Arctic study linking snow cover to discharge, that relies on a precipitation model rather than remote sensing data (Park et al., 2024).

Generally three types of approaches are used to quantify the SWE contribution to river discharge. Firstly, most SWE–discharge studies employ statistical measures of association, mostly correlations or regression approaches, which can only incorporate additional drivers or temporal lags to a limited extent (e.g. Xu et al., 2009; Tong et al., 2010; Biancamaria et al., 2011; Wang et al., 2017; Kumar et al., 2019). Secondly, ratio-based approaches, such as the snow dominance ratio used globally by Barnett et al. (2005) and Gottlieb and Mankin (2024) or regionally by Li et al. (2017), assume total precipitation equals discharge and likewise do not explicitly address storage, evaporation or time lags. Finally, the analysis of stable oxygen isotopes can also distinguish snowmelt contributions in streamflow (Craig, 1961), but its reliance on intensive field sampling limits studies to small catchments (López-Moreno et al., 2023; Lucianetti et al., 2020; Beria et al., 2018).

In sum, no hemispherical scale study currently quantifies snow's role in river discharge composition using multivariate, time-lagged methods (Schilling et al., 2024; Gordon et al., 2022). Also the streamflow seasonality analysis by Han et al. (2024) addresses timing rather than magnitude, and relies on correlational rather than causal methods. This underscores the need for analyses that incorporate time-lagged, storage-sensitive mechanisms.

1.2 Background on Causal Inference in Environmental Science

Causal inference methods are driven by the question: "What effect does a certain trigger variable X have on a target variable Y?" An early attempt to address this question was made by Granger (1969), who introduced the concept of using the unique predictive power of X to identify causal relationships in time series. Later, Spirtes (1996) enabled the analysis of causal relationships along a causal graph. Furthermore, Pearlian approaches expanded this framework to multivariate and lag-specific contexts, allowing tests of conditional independence across time as well as the quantification of the ef-

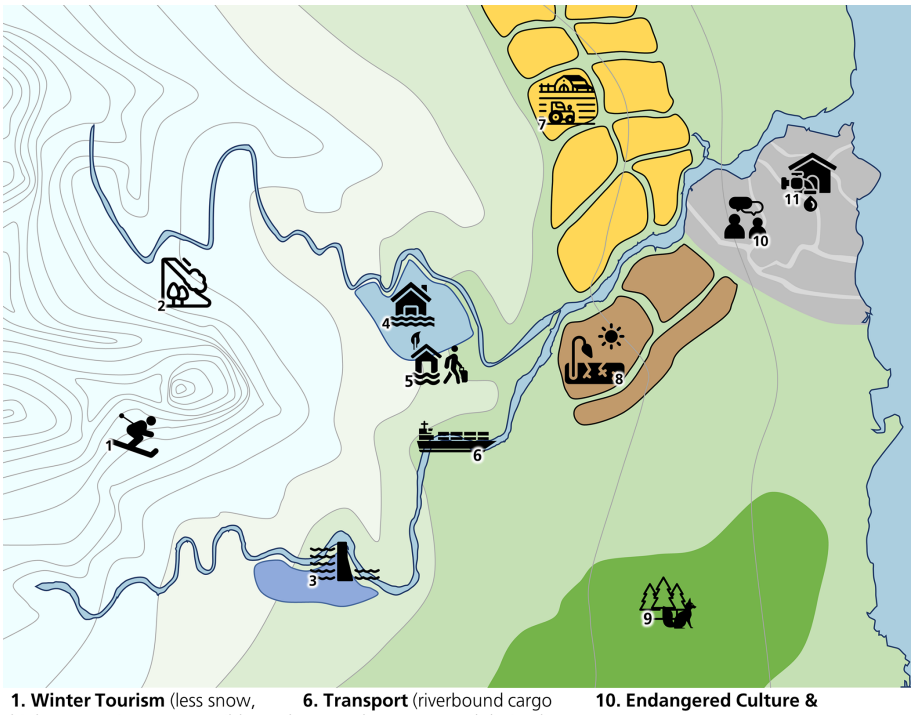


Figure 1. Schematic illustration of the impacts of changing snowpacks.

fect that an intervention X' has on Y (Runge et al., 2012; Pearl, 2000).

In environmental applications, such causal effects are often interpreted in terms of the contribution of individual processes or variables to a system response. In the context of snow hydrology, this naturally raises the question of how snowmelt contributes to river discharge and how this contribution varies across space and time. In this study, we apply a recently developed causal inference method, causal effect discovery, based on Peter Clark Momentary Conditional Independence Plus (PCMCI+) (Runge, 2020), an extension of the original PCMCI algorithm (Runge et al., 2019) described in more detail in Sect. 2.5.1, in combination with the causal effect estimation approach introduced by Runge (2021). Throughout this paper, we use PCMCI to refer to the general family of algorithms and PCMCI+ when referring specifically to the method applied in this study.

While initially developed for economic research (Granger, 1969), causal inference methods have recently gained traction in environmental and Earth observation (EO) studies. Granger causation has been applied in ecological research (e.g. Philippon et al., 2005; Cicuendez et al., 2015; Zhu and Meng, 2015) as well as in broader environmental and climate related studies (e.g. Beyers, 1998; Capua et al., 2020; Pérez Valentín and Müller, 2020). With the development of PCMCI, the scope of causal inference applications in EO studies has further expanded, enabling multivariate and lag aware analyses of complex environmental systems (e.g. Uereyen et al., 2022; Sogno et al., 2024; Karmouche et al., 2023).

Snow-related variables have been incorporated into multivariate environmental systems in a number of studies using causal inference. However, in most of these studies, snow was not the primary focus, but rather one of several variables considered in their causal networks, often without explicitly quantifying its contribution to river discharge or water availability (e.g. Kretschmer et al., 2016; Uereyen et al., 2022; Kolluru et al., 2024; Yuan et al., 2024). Causal studies with a hydrological focus have instead concentrated on specific phenomena such as floods (Sun et al., 2024; Kashyap and Behera, 2024), rain on snow events (Koya et al., 2024), or groundwater dynamics (Zhang et al., 2019). A recent study by Kim et al. (2025) examined the influence of sea surface temperature variability on North American snow resources, but did not explicitly link snow dynamics to downstream hydrological responses. To our knowledge, to date, no large

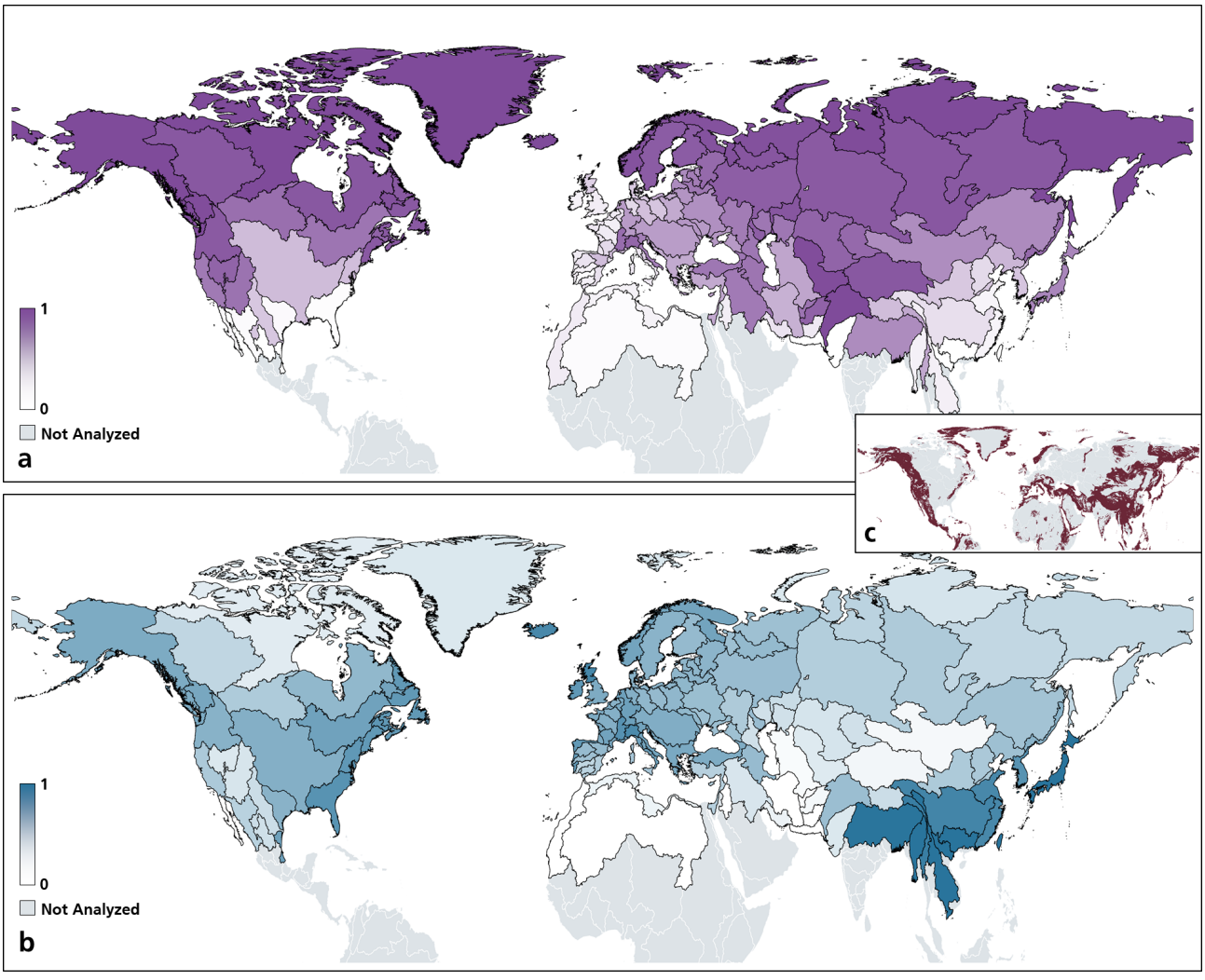


Figure 2. Top **(a)**: Normalized average ratio between snowmelt and total precipitation in the analyzed river basins for 1980–2022 (Data: ERA 5 Muñoz Sabater, 2019), Bottom **(b)**: Normalized average monthly total precipitation (1980–2022) in the analyzed river basins (Data: Era 5 Muñoz Sabater, 2019). Middle right **(c)**: Mountainous areas of the Northern Hemisphere (Data: GMBA Inventory v2.0 Snethlage et al., 2022).

scale causal analysis has specifically examined the contribution of snowmelt or snow water equivalent to river discharge across extended spatial and temporal scales.

Given the demonstrated applicability of PCMCI to environmental time series, it can be considered a suitable framework for addressing this research gap. This study thus presents a hemispherical scale causal inference analysis of snow hydrology, targeting the contribution of snowmelt and rain to river discharge. The analysis incorporates variables beyond snowmelt and river discharge, including rain, soil moisture, evapotranspiration, glacier runoff, baseflow flux, and temperature, while accounting for time lags of up to six months. This is complemented by a descriptive trend analysis of snow water equivalent (SWE) and related variables. The differentiation between snowmelt and SWE across the two analyses reflects their different purposes: the causal inference requires snowmelt as an input to resolve its seasonal contribution to river discharge, whereas the trend analysis uses SWE directly, to remain comparable with existing SWE studies. The choice of a specific causal inference method should reflect the structural properties of the system under study rather than be made by default. A range of approaches exist for identifying causal relationships in multivariate, time-evolving data, including information-theoretic methods such as the Liang-Kleeman information flow (LKIF; Liang and Kleeman, 2005) and constraint-based graphical methods such as PCMCI and PCMCI+ (Runge et al., 2019, 2023). Since our system comprises eight interacting hydrological and atmospheric variables observed across multiple time lags, a method needs to be able to condition on the full set of

common drivers and mediators. Simpler bivariate approaches cannot adequately rule out indirect or confounded links under such conditions. Docquier et al. (2024) systematically benchmarked PCMCI against LKIF across synthetic systems of increasing complexity and a real-world case study and found that, while both methods outperform classical correlation-based analysis, PCMCI performs comparatively better as the number of variables in the system increases. While not a direct validation of our specific setup, this supports our choice to use PCMCI+ as an appropriate framework for the multivariate, hemispherical scale snowmelt-discharge system examined here.

2 Data and Methods

The workflow in this study can be distinguished into three main phases: Downloading and Preprocessing, Statistical Metrics and Trend Calculation, and Causal Inference. In the following section we describe these working phases as well as the utilized data and the study area. A schematic overview of the used data, as well as the workflow is shown in Fig. 3. There is no validation section provided here, as no independent data are available that are both spatially and temporally suitable for the scale of this study. All utilized data, as well as the corresponding updates by the providing entities, were validated by the developers and published in peer-reviewed studies (cited in the corresponding sections), and are thereby meeting the qualitative requirements of the analysis at hand.

2.1 Studied Basins and Period

For the delineation of the hydrological basins we use the "Major Hydrological Basins of the World" dataset from the Food and Agriculture Organization of the United Nations (Food and Agriculture Organization of the United Nations, 2011). The dataset defines basins as top-level drainage areas bounded by topographic divides, within which all surface water flows toward a common outlet such as a river, lake, or ocean (Food and Agriculture Organization of the United Nations, 2011). Based on the ECWMF reanalysis land (ERA 5 Land; Muñoz Sabater, 2019) SWE datasets, we determine the number of years each basin had snow coverage between 1980 and 2022. We select basins that have snow coverage for at least 30 of these 43 years, yielding 119 basins for examination. We focus on the Northern Hemisphere because, although there are snow-dominated regions in the Southern Hemisphere, the majority of the world's SWE, snow-dominated rivers, and thus the human populations affected by the described effects in the introduction, are found in the Northern Hemisphere (Barnett et al., 2005; UN DESA, 2022; Tangdamrongsub et al., 2021). We choose the period from 1980 to 2022 because 1980 marks the beginning of consistent passive microwave satellite coverage, on which the employed soil moisture dataset relies. The extent of the analyzed basins can be seen in the Fig. 2.

2.2 Data

Generally, spatial and temporal considerations guide the data selection. When multiple comparable datasets were available, we select the dataset based on practical handling aspects. For temperature we use ERA5-Land, provided by the European Centre for Medium-Range Weather Forecasts (ECMWF) and available in the Copernicus Climate Data Store (CDS). ERA5-Land is likewise used as the SWE data source, as it was identified as the top-performing product for Northern Hemisphere SWE across a comprehensive range of evaluation metrics in the SnowPEx+ intercomparison by Mudryk et al. (2025), supporting its use as the primary dataset for a hemispheric-scale study. For rain we instead use the coarser-resolution ERA5 product, since ERA5-Land does not provide a precipitation type variable, which is required to separate liquid from solid precipitation (see Sect. 2.3.2). River discharge data were provided by the Global Flood Awareness System (GloFAS), and the soil moisture (SM) data by the European Space Agency (ESA) Climate Change Initiative (CCI), both datasets are also obtained from the CDS. The baseflow flux, which serves as a proxy for groundwater runoff, and the glacier runoff data come from the Modern-Era Retrospective analysis for Research and Applications Version 2 (MERRA 2) provided by the Global Modeling and Assimilation Office (GMAO) of the National Aeronautics and Space Administration (NASA). Finally, for evapotranspiration we use the evapotranspiration variable from the Global Land Evaporation Amsterdam Model (GLEAM) version 4.1, which is maintained by the University of Ghent. For this study, we exclude open-water evaporation from the evapotranspiration variable, since it operates directly at the river surface rather than through terrestrial pathways, and exclude snow sublimation, as its inclusion would contradict the snowmelt definition used here (Sect. 2.3.1). Within this setup, evapotranspiration is expected to influence river discharge indirectly through soil moisture depletion, which is included as a mediating variable in the causal graph (see Appendix A). Table 1 provides a complete overview of the datasets used and their sources.

2.3 Preprocessing

We download all data in the provided temporal resolution and average by calculating the biweekly mean. Spatially we average the data by basin, using a proportional approach to avoid values being attributed to multiple basins. Therefore we overlay the variable data, which are all provided as raster data over the vector geometries of the basins. For all pixels that touch more than one basin, we calculate the share of each basin, and attribute the value accordingly. The individual preprocessing steps applied per variable are described in

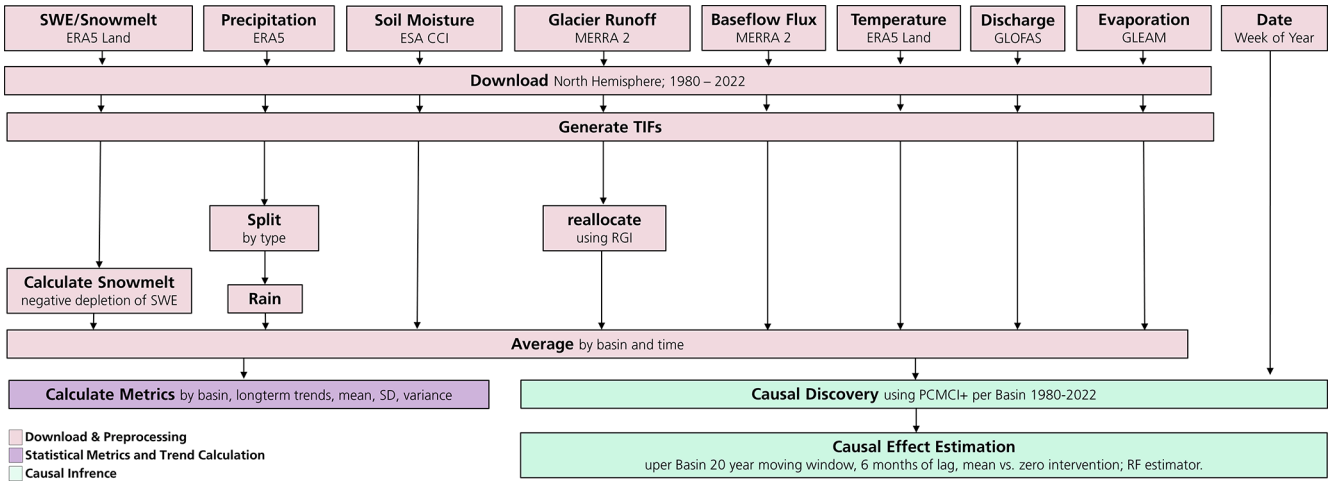


Figure 3. Schematic illustration of the applied data and workflow. Data abbreviations explained in Table 1. Randolph Glacier Inventory (RGI; RGI 7.0 Consortium, 2023) used to reallocate Glacier data if needed.

the following subsections. Note that stationarity is a requirement for PCMCI+ and therefore detrending and a seasonal decomposition of the time series are suggested by Runge et al. (2023). Our objective, however, is to preserve possible long-term trends in the causal factors. We therefore do not detrend the data or subtract a fixed seasonal climatology. Instead, we incorporate a deterministic seasonality variable to allow causal relationships to vary within seasons and repeat the analysis using a sliding window to assess the impact of climate change. This avoids filtering aggregated seasonality and accounts for the potential shift of seasonal patterns under climate change. This approach is described in more detail in Sect. 2.5.1.

2.3.1 SWE/Snowmelt

Since the causal inference focuses exclusively on the snowpack's contribution to river discharge, thus the ablation phase, we use snowmelt as an input variable for the causal inference rather than SWE. Therefore we convert SWE into snowmelt, defined as the depletion of the SWE between successive time steps (Musselman et al., 2017; Wu et al., 2022). For each pixel we calculate the difference in SWE between consecutive time steps and sum all negative changes as absolute values to quantify total snowmelt. This conversion is applied exclusively for the causal inference framework (Sect. 2.5). The descriptive trend analysis of variables (Sect. 2.4) uses SWE directly, without conversion to snowmelt.

2.3.2 Precipitation/Rain

To isolate the liquid fraction of precipitation and thereby avoid conflating precipitation-driven and snowmelt-driven contributions to river discharge, we derive a liquid precipitation dataset, referred to as *rain* throughout this paper, directly from ERA5 total precipitation. We use ERA5 rather than ERA5-Land for this purpose, since ERA5-Land does not provide a precipitation type variable, which is required to separate liquid from solid precipitation. This is done using the precipitation type variable provided by the CDS (Hersbach et al., 2023), which classifies each hourly precipitation value as liquid or solid, of which we only retain the liquid fraction. This classification is applied on an hourly basis before biweekly averaging. Note that rain is derived independently of snowmelt, which is calculated separately from the depletion of snow water equivalent (SWE) as described in Sect. 2.3.1, rather than by subtracting snow-related quantities from total precipitation.

2.3.3 Glacier Runoff

The MERRA-2 data, used for the glacier runoff variable, has a resolution of $0.625° \times 0.5°$ (GMAO, 2015b). This resolution occasionally results in pixels with runoff values touching basins that have no glaciers. In our proportional approach for attributing the pixel values to the basins, glacier runoff would thus be falsely included in the analysis of these basins, if not addressed. To counteract this issue, we identify glacier locations using the Randolph Glacier Inventory (RGI) v7.0 (RGI 7.0 Consortium, 2023). We use spatial overlap analysis to reveal basins which contain no glaciers but have runoff attributed to them and manually reallocate their glacier runoff to reflect hydrological conditions as accurately as possible.

2.4 Statistical Metrics and Trend Calculation

For all data-based variables (see Table 1), we compute a range of statistical measures (mean, median, variance, and standard deviation [StDev]) for each basin to characterize the data distribution and behavior. Note that this trend analysis uses SWE directly, in contrast to the causal inference frame-

Table 1. Data used for the analysis with the corresponding sources. Biweekly averages were used for all datasets.

Variable	Source	Unit	Res.	Data Type	Last Accessed	Remarks
Basin Outlines	FAO Major Hydrological Basins (Food and Agriculture Organization of the United Nations, 2011)	–	–	Vectorized Basin Outlines	Jul 2025	–
Rain	ERA 5; ECMWF (CDS) (Hersbach et al., 2023)	m	0.25°	Reanalysis	Dec 2025	Liquid precipitation classification using the precipitation type variable of ERA 5.
Temperature	ERA 5 Land; ECMWF (CDS) (Muñoz Sabater, 2019)	K	0.1°	Reanalysis	Nov 2025	2 m temperature.
SWE/Snowmelt	ERA 5 Land; ECMWF (CDS) (Muñoz Sabater, 2019)	m	0.1°	Reanalysis	Jun 2026	SWE used directly for descriptive trend analysis (Sect. 2.4); converted to snowmelt, defined as its negative depletion between time steps, for causal analyses (Section 2.3.1).
River Discharge	GloFAS (Grimaldi et al., 2022)	$m^3\ s^{-1}$	0.05°	Reanalysis	Nov 2025	–
Soil Moisture	ESA CCI (Dorigo et al., 2019)	$m^3\ m^{-3}$	0.25°	Passive & Active MW	Nov. 2025	No data days interpolated.
Baseflow Flux	MERRA-2 (GMAO, 2015a)	$m^3\ s^{-1}$	0.5° × 0.625°	Reanalysis	Nov 2025	–
Glacier Runoff	MERRA-2 (GMAO, 2015b)	$m^3\ s^{-1}$	0.5° × 0.625°	Reanalysis	Nov 2025	–
Evapotranspiration	GLEAM v4.1 (Miralles et al., 2025)	mm	0.1°	Model	Dec 2025	–

work described in Sect. 2.5, which uses snowmelt derived from SWE as described in Sect. 2.3.1. Additionally, we apply a Theil-Sen estimator (Sen, 1968) to each variable and basin to estimate trends while minimizing outlier influence. Since the Theil-Sen estimator lacks an inherent significance measure, we combine it with a Mann-Kendall test to evaluate trend significance. We normalize the resulting Theil-Sen slopes in two steps. First, for each basin and variable, the slope is normalized by that basin's own mean of the variable over the full 1980-2022 period, yielding a unitless relative trend that is comparable across variables with different magnitudes and units. Second, for visualization purposes, these basin-normalized trends are additionally normalized across all basins per variable by the maximum absolute value, preserving sign, such that the basin with the most extreme trend is mapped to ± 1. These statistical analyses and trend estimations provide a comprehensive understanding of the data across the study region and support a detailed discussion of causal effects and trends across basins.

2.5 Causal Inference

Our causal inference framework (schematic overview in Fig. 5) consists of two phases: causal discovery and causal effect estimation. The causal discovery phase constrains the causal graph based on a series of unconditional and conditional independence tests. The causal graph describes the relationships between the different variables over the defined time lags. The causal effect estimation phase uses the causal graph to determine the effect that an intervention on a trigger variable has on a target variable (Runge et al., 2023; Pearl, 2000).

We run PCMCI+ once per basin over the entire study period to detect basin-specific relationships between the examined variables. This is possible because we assume that basic hydrological principles remain unchanged for the entire study period. Following causal discovery we perform a series of causal effect estimations on 23 subperiods of 20 years (1980–1999, 1981–2000, …, 2003–2022) for each basin. In addition to enabling the detection of long-term change in

effect size, this moving window design restricts each individual estimation to a shorter temporal period, reducing the influence of long-term trends on the causal effect estimates within any given window. We average the values from the subperiods per year resulting in a 43-year yearly time series of causal effects per basin and trigger variable. The effect estimation is run for the 119 basins mentioned in Sect. 2.1 and for the trigger variables snowmelt and rain, as these variables may be regarded as primary drivers within our assumed system, which subsequently influence all other hydrological variables (DeWalle and Rango, 2008). Our framework addresses non-stationarity without modifying the data in two ways: (1) we address seasonal non-stationarity through the inclusion of a calendar week index as an explicit variable in the causal graph, which relaxes the stationarity assumption to year-to-year rather than across the full record, and (2) we address long-term trends through the rolling window approach, which restricts each estimation to a 20-year period where the trend is small enough to be ignored. We confirmed this using Theil-Sen and Mann-Kendall trend analysis across all 20-year moving windows. Even for variables with a significant long-term trend over the full 43-year record, the vast majority of individual 20-year windows showed no statistically significant trend, and if significant trends were detected, they were confined to specific sub-periods rather than present throughout the record. Since non-stationarity is addressed within the method rather than by preprocessing the data, formal stationarity tests are not applicable in this context.

To confirm the basic functionality of the method, we carry out a set of plausibility checks using artificially modified input data. We apply two mirrored scenarios to the input time series: in the first, a compounding scaling factor artificially increases the snowmelt signal while simultaneously decreasing the rainfall signal. In the second, the opposite scaling is applied. We repeat this check for both trigger variables across a range of basins and consistently find the detected causal effects to respond in the expected qualitative direction. The results for the Danube basin as representative example show the functionality of the method (Fig. 4). The following subsections further describe our application and parametrization of the two causal inference phases on the snowmelt river discharge relationship.

2.5.1 Causal Discovery

For the causal discovery we use PCMCI+ (Runge, 2020; Runge et al., 2023), motivated by the multivariate structure of our system as discussed in Section 1.2. PCMCI+ extends the original PCMCI algorithm (Runge et al., 2019) by additionally enabling the detection of contemporaneous causal links, i.e. causal relationships occurring within the same time step, alongside lagged relationships (Runge, 2020). This extension is relevant for our setup, as some hydrological interactions may occur within a single biweekly time step. The analysis was conducted using the Tigramite Python package (https://github.com/jakobrunge/tigramite, last access: 8 June 2026), which implements both PCMCI and PCMCI+. Our causal discovery is applied to eight biweekly variables obtained from time series data. These are river discharge, snowmelt, rain, glacier runoff, soil moisture, baseflow flux, evapotranspiration and temperature. Additionally, we include the calendar week as an explicit index variable in the causal graph. This relaxes the stationarity assumption underlying PCMCI+ from stationarity across the full 43-year record to stationarity from year to year, thereby accounting for seasonal non-stationarity without requiring the variables to be detrended or deseasonalized prior to analysis. The calendar week variable is used only as a proxy for seasonality in the data, not as a variable with a direct causal effect. It captures the time of year, but should not be interpreted as a mechanistic driver of the hydrological variables studied here. Within PCMCI+ we specify a system of connections among the variables based on established hydrological and atmospheric relationships (DeWalle and Rango, 2008; Tague and Grant, 2009; Huss and Hock, 2018; Hammond and Kampf, 2020; Slater and Binley, 2021). These constraints are implemented as allowed relationships rather than fixed assumptions, restricting the search space without imposing causal links. Some link directions are predetermined by hydrological theory, while others remain unconstrained and are oriented by PCMCI+ using the PC algorithm's orientation rules. A schematic illustration of the assumed hydrological system is provided in Appendix A. The PCMCI+ algorithm consists of two substages. Firstly, the Peter Clark (PC) algorithm builds a causal graph based on two key assumptions: the Markov condition (dependence implies connection) and the faithfulness condition (conditional independence implies no direct causation). Variables without unconditional dependencies are removed, after which the algorithm iteratively tests the remaining links for conditional independence, eliminating those that become independent once the common drivers and mediators are accounted for (see Fig. 5A, green arrow). This procedure continues until no further tests are possible, yielding the set of candidate parents (Runge et al., 2023, 2019). Secondly, the Momentary Conditional Independence (MCI) test evaluates the candidate parents using an expanded conditioning set (see Fig. 5A,blue arrow). By conditioning on the lagged parents of the driver and target variables, MCI refines the causal graph and reduces autocorrelation effects (Runge et al., 2023, 2019). The conditional independence test for PCMCI+ can be adapted for the research problem at hand. We use the Conditional Mutual Information (CMIknn), as a conditional independence test, as it does not assume any parametric form for the relationship between variables (Runge, 2018). This was crucial, given the presence of nonlinear relationships in our system.

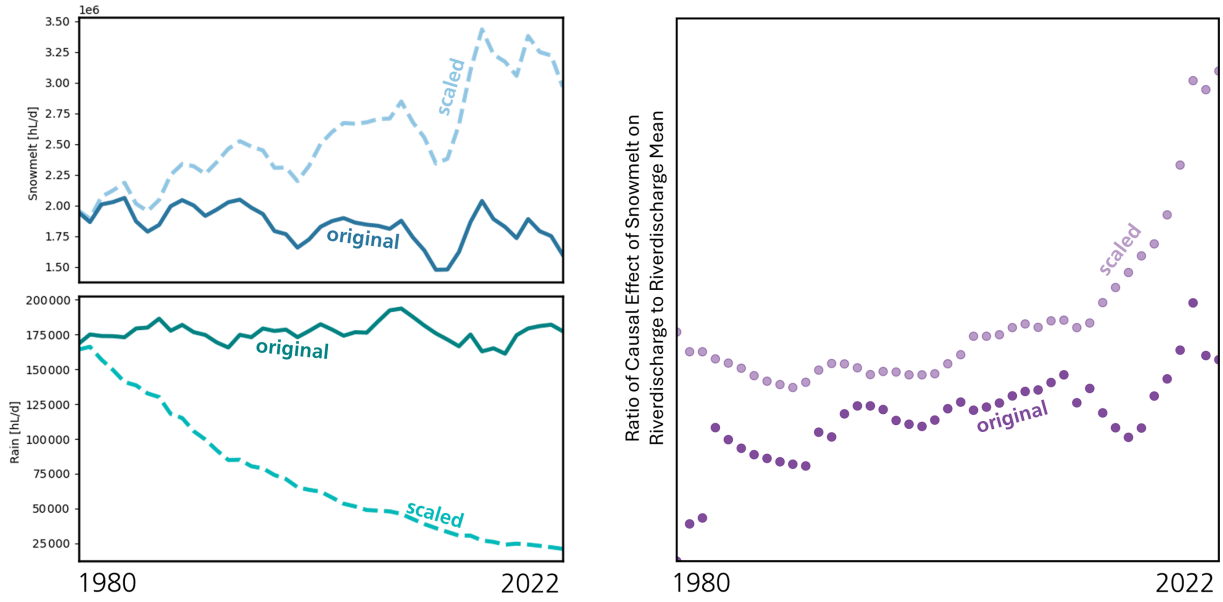


Figure 4. Plausibility check results for the Danube basin, shown here as a representative example, using artificially modified snowmelt and rain input signals. The causal effect of the amplified trigger variable increases and the causal effect of the attenuated trigger variable decreases under each scenario, confirming that the detected causal effects respond in the expected qualitative direction to changes in the underlying input signals.

2.5.2 Causal Effect Estimation

While the causal graph reveals the presence and direction of causal effects between variables over time, it does not quantify the strength of these effects. To estimate the magnitude of the causal relationships, causal effect estimation is conducted (see Fig. 5B). We identify the causal effect via the adjustment formula $E[Y|\mathrm{do}(X)] = \sum_Z E[Y|X,Z]\,P(Z)$ (Pearl, 2000; Runge, 2021), where Y is the target variable (river discharge), X is the trigger variable (snowmelt or rain), and Z denotes the adjustment set identified from the causal graph. The random forest (RF) estimator is used solely as a non-parametric parametrization of the conditional expectation $E[Y|X,Z]$, not as a causal model itself (Breiman, 2001; Geurts et al., 2006). It is trained to predict river discharge given the trigger variable and the adjustment variables simultaneously. We use an RF estimator for this purpose to account for the versatile, non-linear nature of the relationships examined in this study, since the RF does not presume the type of relationship between two variables. Once fit, the causal effect is computed as the difference between model predictions under two different interventions on X (described below), evaluating the identified quantity $E[Y|\mathrm{do}(X)]$ rather than reflecting model sensitivity. Because X influences Y both directly and indirectly, through mediating variables and across multiple time lags (see Fig. 5A), the resulting causal effect corresponds to the sum of path coefficients across all lags in the causal graph. It thus reflects the net effect of a unit change in the trigger variable on annual streamflow, integrated over the full lag structure. This combines both short-run and longer-run, potentially opposing, contributions into a single interpretable quantity. While Fig. 5 provides a schematic overview of the overall framework, Fig. 6 illustrates the underlying mechanics of the causal inference workings in more detail, walking through the causal graph, query, the resulting adjustment set, the random forest, and the resulting effect estimate for an example basin. We configure the RF with 1000 estimators to enhance model robustness, using the absolute error criterion to make the model more sensitive to small deviations in the data. To avoid overfitting, the maximum depth is set to 10, as this value results from a global hyperparameter search in which different tree depths were evaluated across all basins and time periods.

Since the resulting effect estimates are directly shaped by how the intervention is defined, the intervention in our causal effect estimation setup has to remain within the support of the observed data, so that the resulting estimate is not driven by model extrapolation. Our basins vary in location, topography, and climate. This means the method must also be comparable across basins. Therefore, in our setup the intervention is not a single global value, but is based on the seasonal structure of each basin and the specific time lag under investigation. For each basin and year, we divide the variable time series into 26 parts, representing the seasonal cycle of the year. For each of these 26 parts, we compute the mean (μ) and standard deviation (σ) of the trigger variable (snowmelt or rain) across all years within the corresponding window. We define two interventions per seasonal block: $\mathrm{do}(X = \mu)$, representing typical conditions, and $\mathrm{do}(X = \mu - \sigma)$, representing reduced snowmelt or rainfall conditions consistent

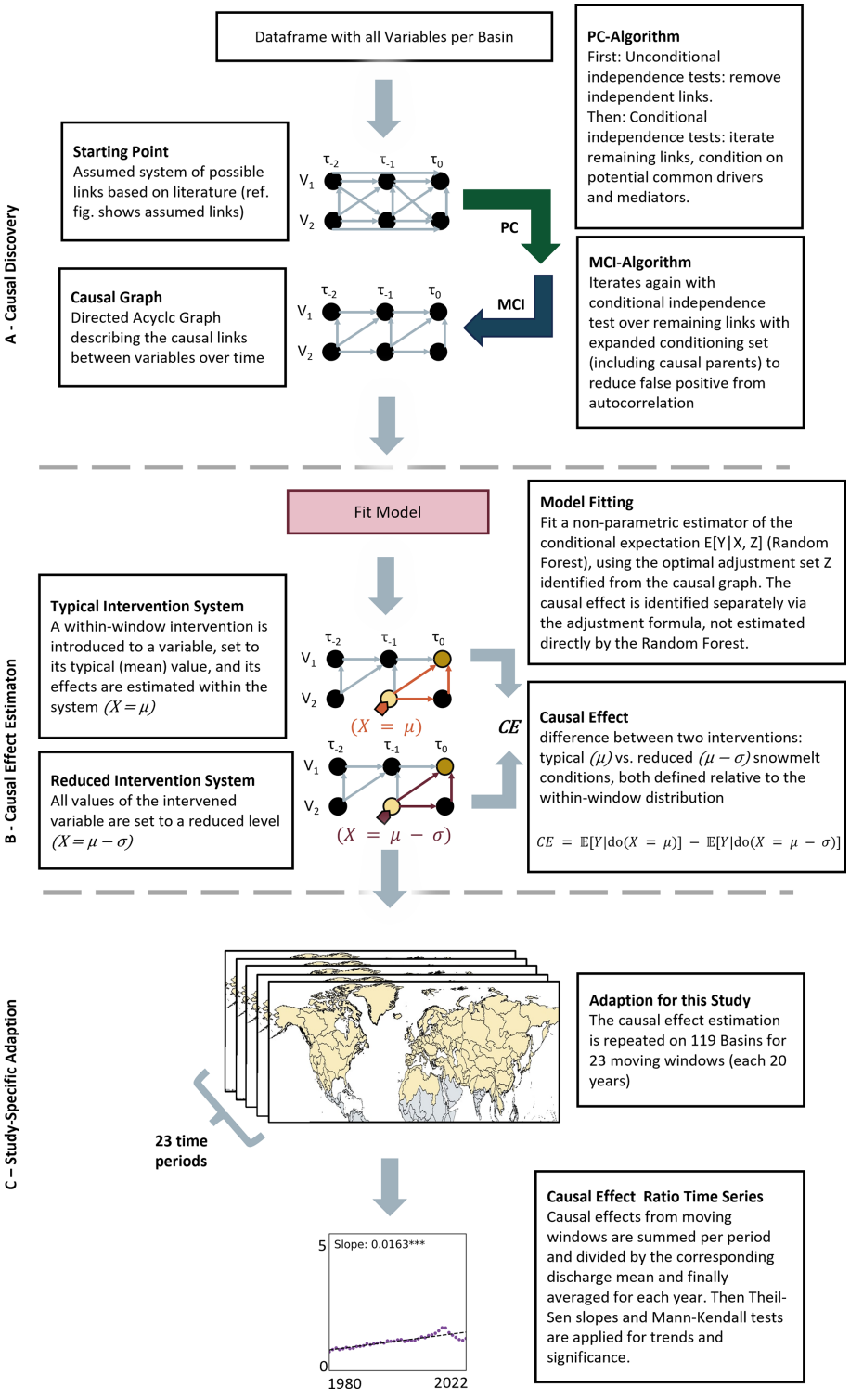


Figure 5. Schematic illustration of the causal inference framework applied in this study. **(A)** Causal Discovery; PC and MCI algorithms examine statistical conditional independences of relationships between variables, which in turn are used to draw the causal graph. **(B)** Causal Effect Estimation; The causal model is fit to the input data, and then two systems, one intervened with $\mathrm{do}(X = \mu)$ and one intervened with $\mathrm{do}(X = \mu - \sigma)$, representing typical and reduced trigger-variable conditions respectively, are compared. The difference between the value of the two systems is the causal effect. **(C)** Study Specific Adaption; Causal effects are estimated in 20-year moving windows across the 43-year time series, allowing the derivation of a causal-effect time series and its trend.

with projected reductions in snowpack under climate change. Both interventions remain within the support of the observed data, avoiding the extrapolation issues associated with a zero intervention. Since the resulting causal effect thus depends both on how strongly discharge responds to the trigger variable and on the magnitude of the anomaly used in the intervention, we additionally report σ itself as a measure of anomaly magnitude, and the ratio $\beta = \mathrm{CE}/\sigma$ as an isolated measure of the coupling strength between the trigger variable and discharge, independent of anomaly magnitude. This decomposition allows us to distinguish whether a trend in the causal effect reflects a change in how strongly the trigger variable itself deviates from typical conditions, a change in how discharge responds to a given deviation, or both. We ensure that these block-specific interventions and the responses of the target are associated with the seasonal block they represent by additionally fixing, rather than causally intervening on, the index variable (calendar week) to the corresponding value. This way the interventions and responses are anchored in time and correctly aligned with each seasonal block.

We run the causal effect estimation for two variables. Firstly to estimate the causal effect of snowmelt on river discharge and secondly to estimate the causal effect of rain on river discharge. For both snowmelt and rain we use the same methodological setup. The causal effect estimation is run using a 20 year moving window, over our 43 years of data. For every period used, we determine the interventions separately using the corresponding time series. This 20-year window size balances the need for sufficient data points to reliably estimate causal effects with limiting the degree of temporal autocorrelation introduced by overlapping windows; a 30-year window, for instance, would result in 29 of 30 years overlapping between adjacent windows. Multiple window sizes were evaluated during development, and 20 years was selected as an appropriate compromise between these two considerations. We then calculate the causal effect as the difference between the model prediction under the $\mathrm{do}(X = \mu)$ intervention (Fig. 5B, orange arrows) and the prediction under the $\mathrm{do}(X = \mu - \sigma)$ intervention (Fig. 5B, dark red arrows). This yields a total causal effect per 20 year period, which we then divide by the mean river discharge of the corresponding 20 year period. We average these effects by year, which results in a 43 year time series (Fig. 5C). Finally, we apply a Theil-Sen estimator together with the Hamed-Rao test, an extension of the Mann-Kendall test that accounts for autocorrelated data (Hamed and Ramachandra Rao, 1998), per basin and target variable. If in a basin at least one yearly average is zero, we exclude the basin from the trend analysis, as zeros near the edges of the time series can lead to unstable or notably steep trend slopes.

3 Results

3.1 Variable Trends

The normalized Theil-Sen trends of all variables in the analyzed basins, computed as described in Sect. 2.4, are illustrated in Fig. 7. A selection of basins, together with the corresponding causal trends, is examined in more detail in Sect. 3.4. As a comprehensive discussion of all variables and basins is beyond the scope of this publication, the full set of statistics per basin is provided in the supplementary materials (Appendix B).

Figure 8 contains the same information as Fig. 7. However, the basins are grouped by their river discharge, snow, and rain trend slopes, to generate a general impression of the dynamics in the basins. Note that for visualization purposes we refrained from generating intermediate categories. Therefore, minor and non-significant trends were also considered for the grouping. Even though eight groups are possible, there are four groups to which a majority of the analyzed basins can be attributed (105/119). Fifty-two basins saw a decreasing trend for river discharge, SWE, and rain (purple). An additional twelve basins saw a decrease in river discharge and SWE but an increase in rain (green). This contrasts with 28 basins where the SWE decreased but rain and river discharge increased (orange). Finally the group where river discharge and rain were decreasing comprises 13 basins (blue). Considering these groups, the data furthermore suggests that in nearly all Arctic and Pan-Arctic basins, with the exception of the Yenisey Basin, the SWE was decreasing while rain was increasing, with various outcomes on the river discharge. Also, in the latitude band south of the Arctic, between around 60 and 20° N, a predominant majority of basins saw a decreasing trend in all three variables considered for the grouping.

3.2 North Hemisphere Causal Trends

The causal effect trends for snowmelt and rain on river discharge were assessed across all 119 basins, as shown in Figs. 9 and 10 respectively. Areas colored in light brown were examined but no causal link, effect, or trend could be derived. This does not imply that no connection exists between the trigger variables (snow and rain) and the target variable (river discharge), or that no trend is present, but rather that our setup could not detect a connection, or the basin was excluded due to years with zero values. A positive trend means that the causal effect of snowmelt (or rain) on river discharge increases over time, so that variations in river discharge are increasingly linked to variations in snowmelt (or rain). A negative trend means the opposite. The sign of the trend therefore describes the change in the causal effect and not the change in the variables themselves. For the causal effect of snowmelt on river discharge, our method detected a continuous trend in 73 basins. Of these, 60 had a positive trend,

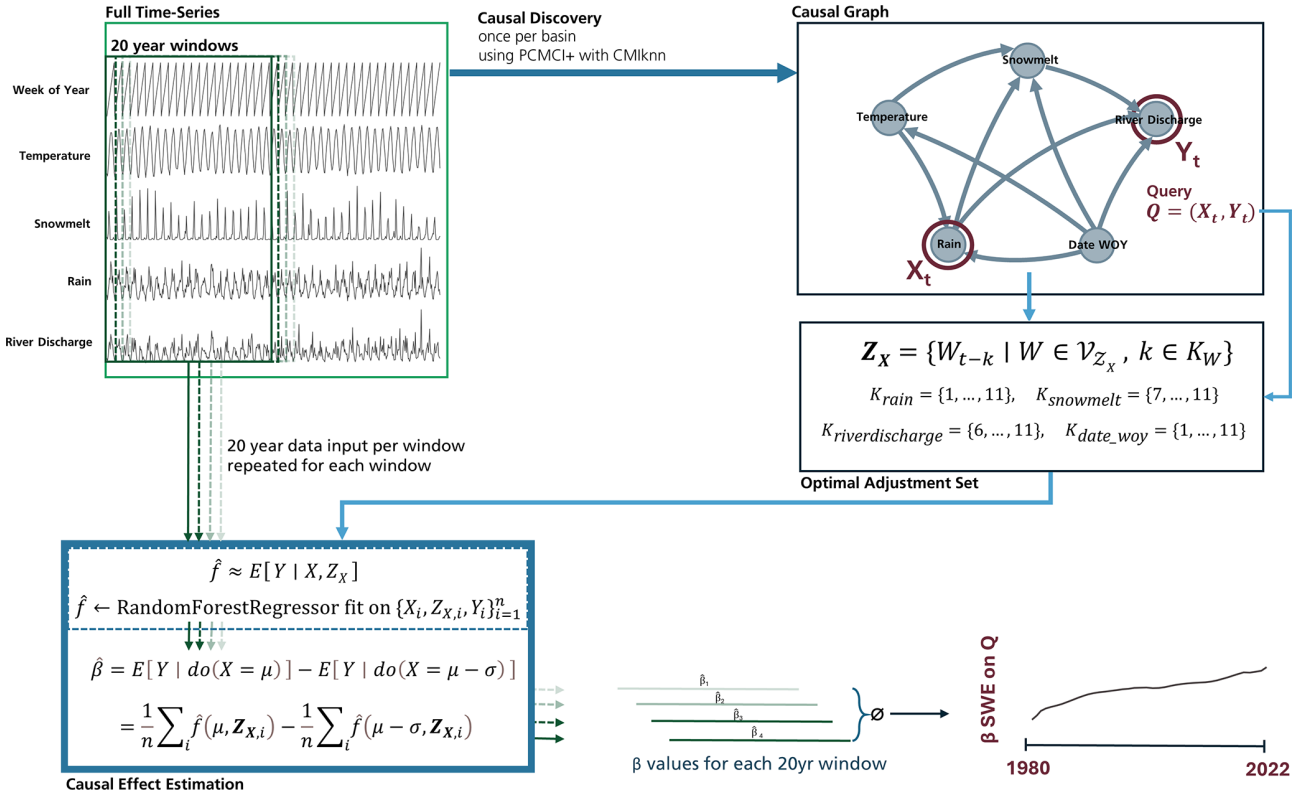


Figure 6. Illustration of the causal effect estimation procedure for an example basin: the causal graph identified during causal discovery with its lag structure, the resulting adjustment set Z for the trigger variable snowmelt, and the intervention design comparing $\mathrm{do}(X = \mu)$ and $\mathrm{do}(X = \mu - \sigma)$. The reported causal effect corresponds to the sum of path coefficients across all lags shown here.

12 of which were significant. For the causal effect of rain on river discharge, the method detected a continuous effect and therefore trend in 114 basins. The effect of rain on river discharge was positive in 67 basins (51 significant), and negative in 47 basins (31 significant). The largest increase for the causal effect of snowmelt on river discharge was found in the Columbia basin (USA and Canada). In contrast, the steepest decrease in the causal effect of snowmelt on river discharge occurred in the Ziya He Interior basin in China. For rain the corresponding extreme values were found in the Lena basin in Russia (steepest increase), and in the Sweden basin (steepest decrease). As the majority of basins showed a positive causal trend for snowmelt, as was also the case for rain, no apparent overarching correlations or patterns emerged, neither for trend direction nor trend magnitude. Thus, no latitude or mountain effect could be observed when correlating the trend slope with the corresponding data. Furthermore, no correlation to the snow dominance (compare Fig. 2) or the overall discharge of the corresponding rivers could be identified. All results and trends can be found with the variable trends, grouped by basin, in Appendix B.

To better understand the drivers behind these causal effect trends, we examine two components separately: how strongly the trigger variable itself deviates in a poor snowmelt or rain year compared to a typical year (the anomaly magnitude), and how strongly river discharge responds to a given anomaly (the sensitivity, independent of how large that anomaly is, called coupling strength). For snowmelt, the anomaly magnitude increased in nearly all basins (72 of 73, 15 significant), whereas the coupling strength of discharge to snowmelt showed no consistent direction, increasing in 27 basins and decreasing in 42 (12 vs. 24 significant, respectively). For rain, the anomaly magnitude increased in every basin (118 of 118, 113 significant), while coupling strength again showed no consistent direction, increasing in 47 basins and decreasing in 62 (27 vs. 41 significant, respectively). This suggests that the predominantly positive causal effect trends for snowmelt, and the majority of positive trends for rain, are mainly driven by growing anomalies in snowmelt and rain themselves, rather than by river discharge becoming consistently more sensitive to them.

3.3 Using Causal Effects as Indicators of Water Stress

One reason to study the relationship between SWE and river discharge, or other measures of water availability, is the increasing occurrence of droughts and snow droughts due to climate change (Cowherd et al., 2023; Gottlieb and Mankin,

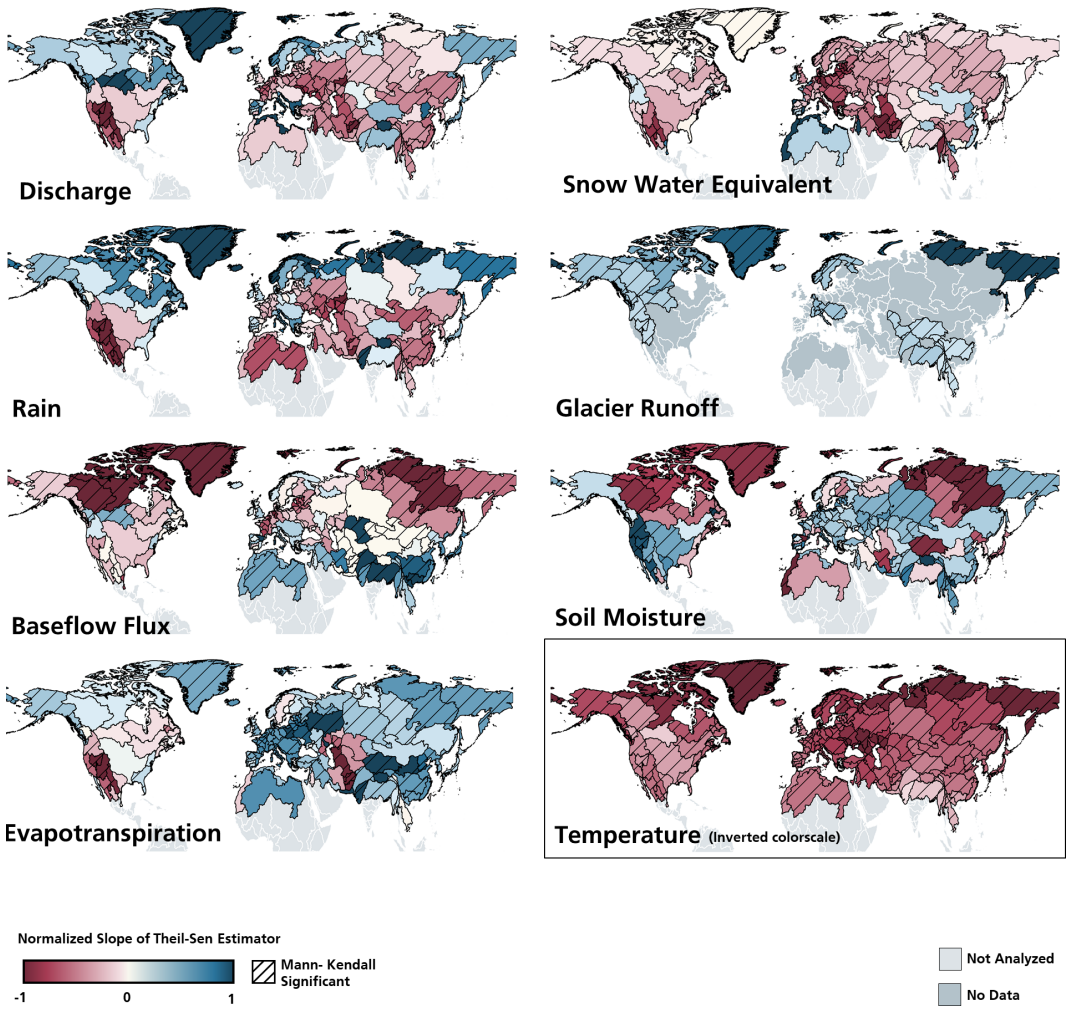


Figure 7. Normalized Theil-Sen trend with Mann-Kendall significance for the period 1980–2022 over all utilized variables in the 119 analyzed river basins. The color scale for all plots is scaled using the 5 % and 95 % percentile to ensure comparability between the different variables). The colorscale for the temperature is inverted.

2024). Identifying regions where SWE is declining alongside river discharge, can therefore indicate where snow loss is a key driver of water stress, given the degree of snow dominance in those basins. Relying on the variable trends of SWE and river discharge, we used our results to identify such regions in our scope. A majority of the basins with a negative discharge trend also have a negative SWE trend (64/79). The remaining 15 basins that show a negative discharge trend despite an increasing SWE trend are shown in light green in Fig. 11. However, apart from the Fraser basin (USA/Canada), these all are located in rain-dominated or very arid regions. In 45 of the 64 basins with decreasing discharge and decreasing SWE our method was able to identify a causal trend. Of those 38 showed an increasing causal effect trend (blue in Fig. 11). In another 7 basins the causal effect of snowmelt on river discharge was decreasing (red in Fig. 11). In these 38 basins, SWE and river discharge both decline, while the causal effect of snowmelt on river discharge increases. River discharge is thus increasingly influenced by snowmelt, even though the snow resource is shrinking and discharge is already decreasing. Therefore, declining discharge points to drier conditions and thus water stress, and the increasing causal effect of snowmelt indicates that this water stress appears to be increasingly snow-driven. In the 7 basins with a decreasing causal effect, discharge declines although its link to snowmelt weakens.

3.4 Exemplary Basins Analysis

As an analysis of all examined basins would fall outside the scope of this publication, we selected six basins on three continents for an exemplary analysis in this section. The basins can all be attributed to the three main groups setup in Sect. 3.1. Figure 12 shows an overview of the course of the causal effects of snowmelt and river rain on river discharge, from 1980–2022 for the exemplary basins. We selected the basins

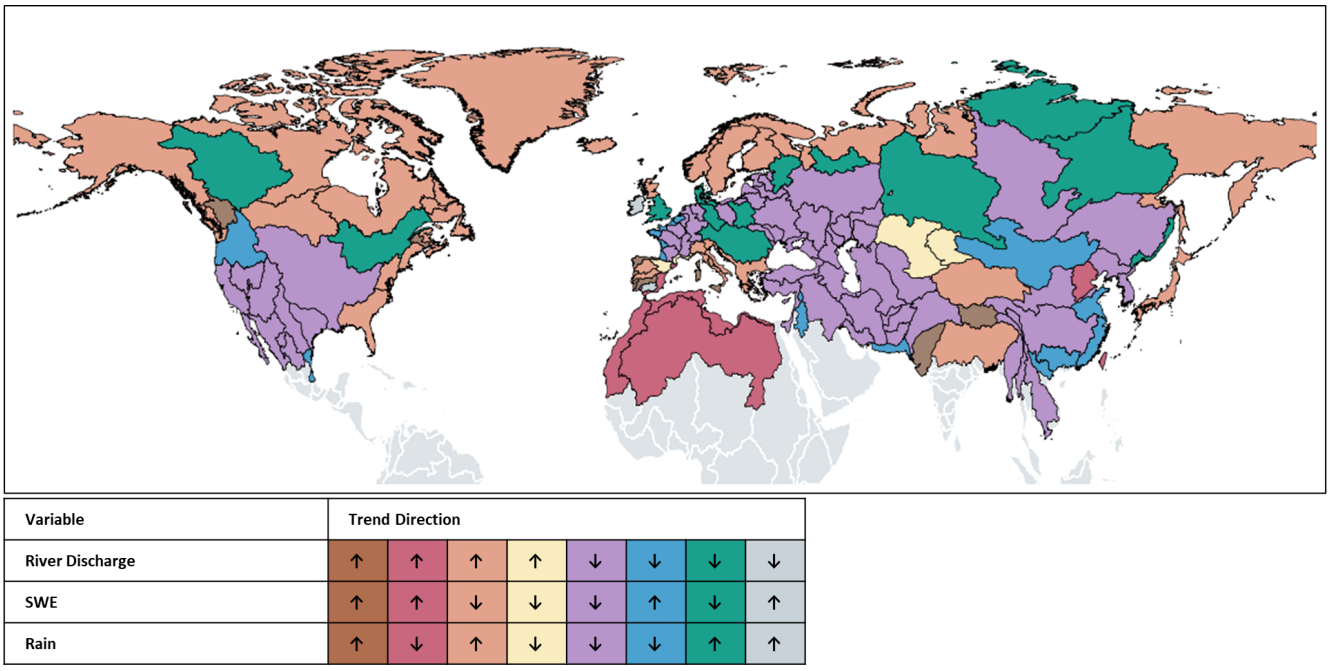


Figure 8. The 119 analyzed river basins, categorized by their river discharge, snow, and rain trend slopes and indicated by the different colors.

based on location, their classification in Sect. 3.1, and the dynamics among the variables. Note that some basins span over multiple climate zones and encompass several land-cover types, as well as subbasin dynamics. Therefore, the analysis of the basin might fall short of explaining the complete range of mechanisms and developments that took place within the basin region during the study period. In the following, a positive trend denotes an increasing causal effect and a negative trend a decreasing causal effect.

3.4.1 Mackenzie

The Mackenzie basin is located in northern Canada and mainly characterized by a subarctic climate (Beck et al., 2023). The basin extends approximately from 52 to 69° N, contains two major lakes (Great Bear Lake, Great Slave Lake) and is primarily dominated by tundra and taiga land cover types (Friedl et al., 2019). Generally the discharge in the Mackenzie basin is mainly snow dominated (Woo et al., 2018), and while glacier runoff plays a role as well it appears to be less dominant as in other, more coastal basins adjacent to the Rocky Mountains (Clarke et al., 2015). In our categorization (Fig. 8), the basin shows a decreasing SWE trend alongside an increasing rain trend, resulting in an increasing discharge trend. However, these trends are relatively stable. In contrast, glacier runoff has increased significantly over the study period, indicating that glaciers are melting and their storage capacity is diminishing. Additionally, both baseflow flux and soil moisture trends are significantly negative. The causal effect of snowmelt on river discharge showed a positive trend (increasing causal effect) in the Mackenzie basin. This coincided with a growing snowmelt anomaly, while the responsiveness of river discharge to snowmelt itself decreased significantly, suggesting that the growing anomaly, rather than a stronger coupling between snowmelt and discharge, drives this trend. For rain, the causal effect on river discharge showed a negative trend (decreasing causal effect), even though the rainfall anomaly grew significantly as well. Here the responsiveness of discharge to rain decreased significantly, which appears to outweigh the growing rainfall anomaly and drive the observed decrease.

3.4.2 Colorado

The Colorado stretches from 32 to 43° N over the southwestern United States and northern Mexico. Despite the mountains in the northeast, the basin generally has an arid climate (Beck et al., 2023), and is mainly covered by grass-, and shrublands (Friedl et al., 2019), as well as extensive agriculture areas (Norton et al., 2021). In the Colorado basin, both snow and rain have declined, corresponding with the observed decrease in river discharge. For snowmelt, the causal effect on river discharge showed a positive, non-significant trend (increasing causal effect), coinciding with a significant increase in the snowmelt anomaly, while the responsiveness of discharge to snowmelt decreased significantly, suggesting that a weakening coupling between snowmelt and discharge counteracts, but does not outweigh, the growing anomaly. For rain, the causal effect on river discharge showed a significant positive trend (increasing causal effect), coinciding

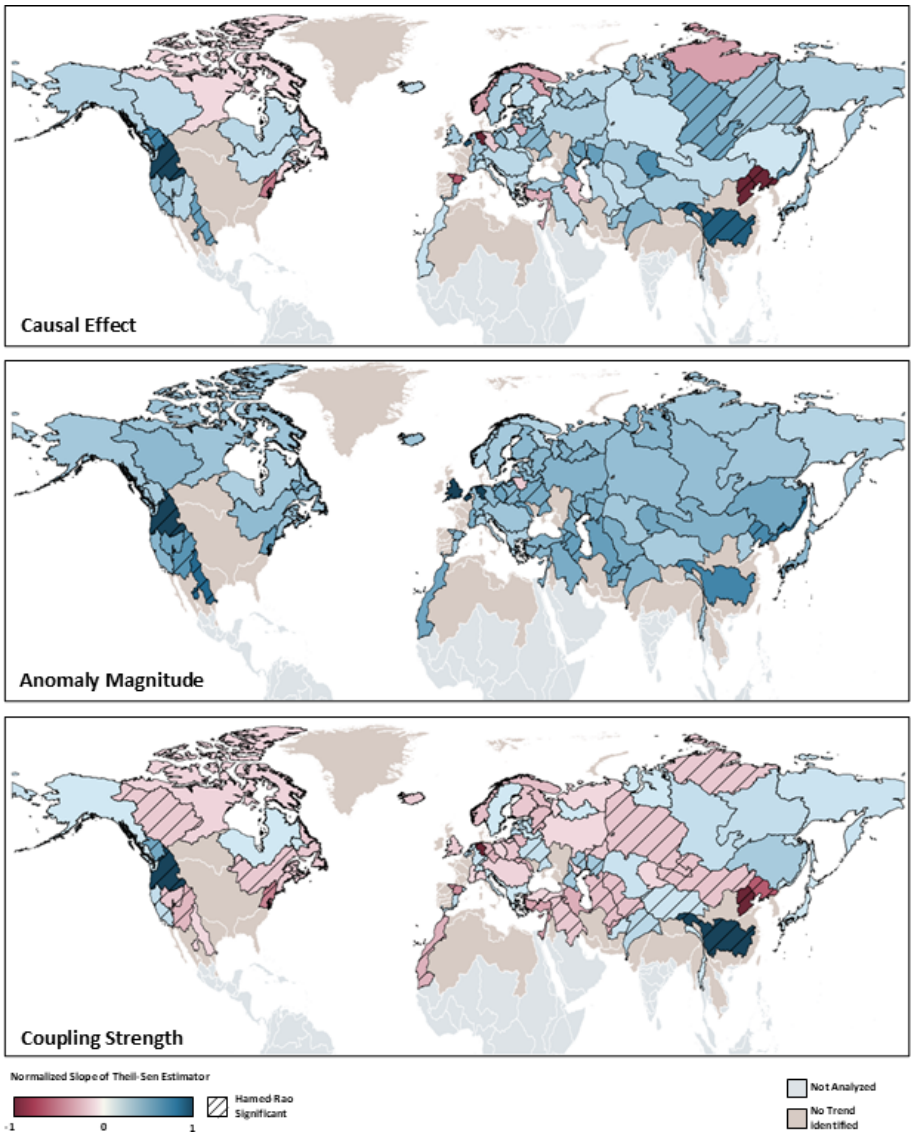


Figure 9. Normalized Theil-Sen trends with Hamed-Rao significance for the causal effect of snowmelt on river discharge between 1980 and 2022, decomposed into three components (top to bottom). Causal Effect: $\mathrm{CE} = E[Y|\mathrm{do}(X = \mu)] - E[Y|\mathrm{do}(X = \mu - \sigma)]$, normalized by mean river discharge, where Y is river discharge and X is snowmelt. Anomaly Magnitude: the trigger-variable anomaly σ used in the intervention, normalized by mean river discharge, reflecting how strongly snowmelt deviates in a poor snowmelt year relative to a typical year. Coupling Strength: $\beta = \mathrm{CE}/\sigma$, the isolated response of discharge per unit of snowmelt anomaly, independent of anomaly magnitude.

with a significant increase in the rainfall anomaly, while the responsiveness of discharge to rain decreased, indicating that the growing rainfall anomaly, rather than a stronger coupling, drives this trend.

3.4.3 Danube

The Danube is the largest river basin in central Europe, following an eastward course reaching from the Alps (8° E) to the Black Sea (45° E) and lying in between 42 and 52° N. The climate is mainly humid in the North of the basin and subtropical in the south, with some arid steppes in the east (Beck et al., 2023). The basin is located over a series of highly populated and industrialized regions, and generally covered with either forest, or grass- and croplands (Friedl et al., 2019). In the Danube SWE was decreasing, rain was increasing, and discharge was decreasing slightly. For snowmelt, the causal effect on river discharge showed a positive trend (increasing causal effect), coinciding with an increasing snowmelt anomaly, while the responsiveness of discharge to snowmelt decreased, though neither of these trends was significant. For rain, the causal effect on river discharge showed a negative trend (decreasing causal effect), coinciding with a significant increase in the rainfall anomaly, alongside a decrease in the

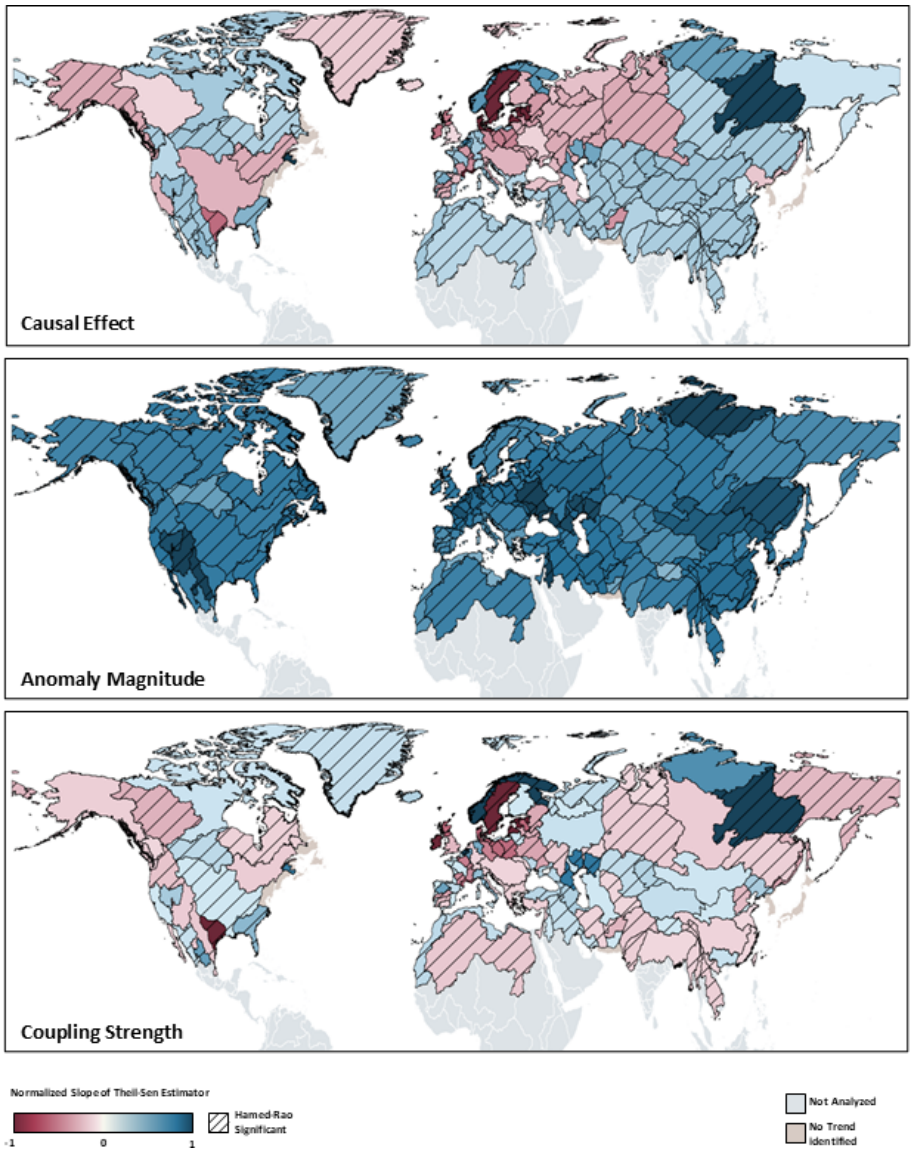


Figure 10. Normalized Theil-Sen trends with Hamed-Rao significance for the causal effect of rain on river discharge between 1980 and 2022, decomposed into three components (top to bottom). Causal Effect: $\mathrm{CE} = E[Y|\mathrm{do}(X=\mu)] - E[Y|\mathrm{do}(X=\mu-\sigma)]$, normalized by mean river discharge, where Y is river discharge and X is rain. Anomaly Magnitude: the trigger-variable anomaly σ used in the intervention, normalized by mean river discharge, reflecting how strongly rain deviates in a poor rain year relative to a typical year. Coupling Strength: $\beta = \mathrm{CE}/\sigma$, the isolated response of discharge per unit of rain anomaly, independent of anomaly magnitude.

responsiveness of discharge to rain, though neither of these last two trends was significant, suggesting that the growing rainfall anomaly outweighs any change in coupling in driving the negative trend.

3.4.4 Po

The Po basin is one of the smallest basins in the analysis, located south of the Alps in mainly northern Italy and to a small part in southern Switzerland between 44 and 46° N. It is characterized by alpine climate in the north and a humid climate in the rest of the basin (Beck et al., 2023). The basin is predominantly characterized by croplands, with occasional forests and major cities such as Milan or Torino (Friedl et al., 2019). The trends for river discharge, and SWE are decreasing, while the rain trend is increasing. The trends, for soil moisture and baseflow flux are contrary to each other, but in a comparatively flat nature. For snowmelt, the causal effect on river discharge showed a slight positive trend (slightly increasing causal effect), coinciding with a slight increase in the snowmelt anomaly and a slight decrease in the responsiveness of discharge to snowmelt, though none of these trends were significant. For rain, the causal effect on

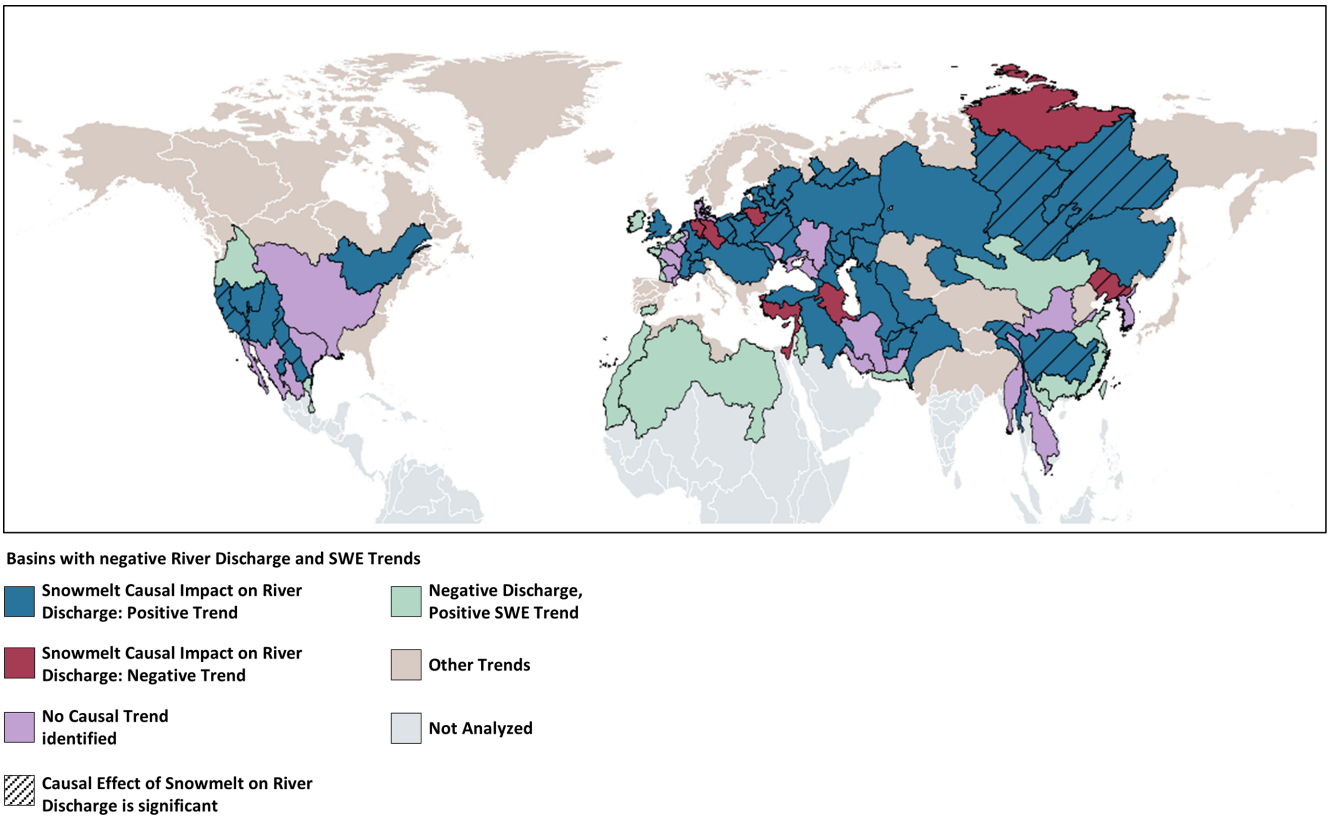


Figure 11. Basins with negative river discharge and negative SWE trends, classified by the trend in the causal effect of snowmelt on river discharge. Blue basins show a positive trend (increasing causal effect), red basins show a negative trend (decreasing causal effect). Purple basins have no causal trend identified. Light green basins show a negative discharge trend despite an increasing SWE trend. Causal effect trends were not analysed for these basins in this figure.

river discharge showed a significant positive trend (increasing causal effect), coinciding with a significant increase in the rainfall anomaly and a significant increase in the responsiveness of discharge to rain, indicating that both the growing anomaly and a strengthening coupling between rain and discharge contribute to this trend.

3.4.5 Yenisey

Reaching, from arid steppes in Mongolia (46° N) over subarctic climate with tundra and taiga to the estuary into the Kara Sea in Siberia/Russia (71° N), the Yenisey basin is fairly diverse and the largest one in this exemplary analysis. In the Yenisey basin river discharge, SWE, and rain all experienced negative trends from 1980 to 2022, whereby the trends for river discharge and SWE are steeper and significant, while the rain trend is only subtly negative and not significant. Both, the causal effect of snowmelt and rain on river discharge were increasing slightly over the study period. For snowmelt, the causal effect on river discharge showed a significant positive trend (increasing causal effect), coinciding with a positive trend in the snowmelt anomaly and a positive trend in the responsiveness of discharge to snowmelt, indicating that both the growing anomaly and an increasing coupling between snowmelt and discharge contribute to this trend. For rain, the causal effect on river discharge showed a significant positive trend (increasing causal effect), coinciding with a significant increase in the rainfall anomaly, while the responsiveness of discharge to rain showed a non-significant negative trend, suggesting that the growing anomaly, rather than a stronger coupling, drives this trend.

3.4.6 Indus

Among others, the Indus Basin is home to some of the tallest mountains in the world (e.g. K2 and Nanga Parbat) and is highly glacierized with some of the world's largest non-polar glaciers (e.g. Siachen Glacier). The basin which is located between 23° N/66° E and 38° N/83° E, is climatically very diverse, reaching from mountain climate in the north, subtropic and savannah climate in the central basin and hot arid desert climate in the south (Beck et al., 2023). The land cover is similarly diverse with the mountains in the north, a mix of grass- shrub- and croplands in the center and along the Indus river itself, and barren deserts in the southeast (Friedl et al.,

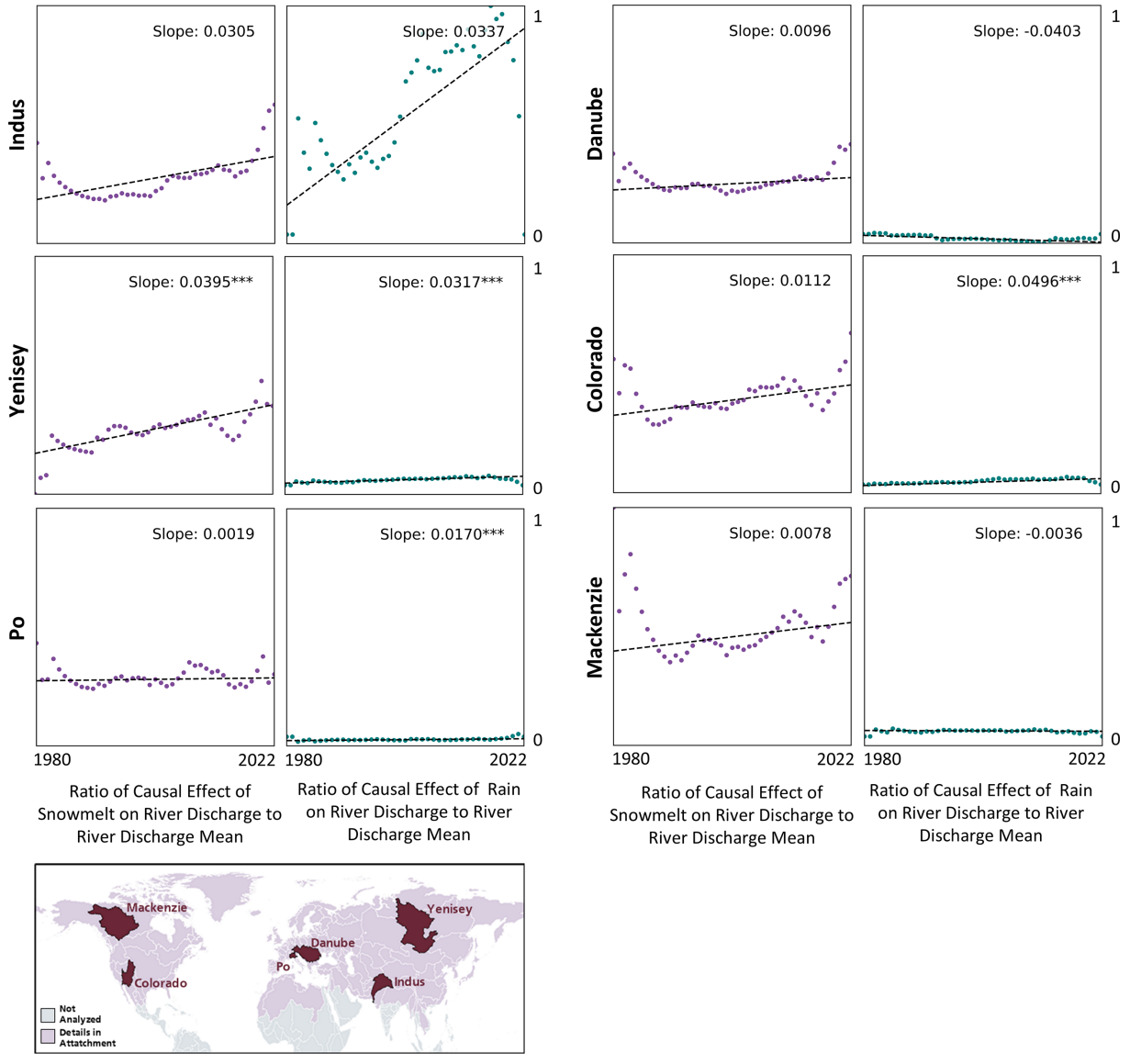


Figure 12. The causal effect of snowmelt on river discharge (both columns on the left – purple) over the examined time period and the six exemplary basins. Causal effect of rain on river discharge (both columns on the right – teal) over the examined time period and the six exemplary basins. Displayed as a ratio of causal effect to mean discharge. Significant (Hamed-Rao test) trends, assessed at the 95 % confidence level ($p < 0.05$) are indicated with asterisks (***). The dots mark the average values per year, the dashed black line marks the Theil-Sen slope per basin. The exemplary basins are marked on the map.

2019). The Indus basin has seen a significant decrease of SWE, discharge, and a non-significant decrease of rain. All these trends are, if not all significant, of a medium steepness in the global comparison. For snowmelt, the causal effect on river discharge showed a positive, non-significant trend (increasing causal effect), coinciding with a non-significant increase in the snowmelt anomaly, while the responsiveness of discharge to snowmelt showed a significant positive trend, suggesting that an increasing coupling between snowmelt and discharge contributes to this trend more than the anomaly itself. For rain, the causal effect on river discharge showed a positive, non-significant trend (increasing causal effect), coinciding with a significant increase in the rainfall anomaly, while the responsiveness of discharge to rain showed a significant negative trend, suggesting that the growing anomaly, rather than a stronger coupling, drives this trend, despite the weakening coupling between rain and discharge.

3.5 Consistency and Fluctuations of Trends

This section assesses the internal consistency of the causal effect estimates: specifically, whether the estimated causal effects are stable within individual basins over time, or

whether they are dominated by noise rather than reflecting a genuine underlying signal. This is distinct from a validation of the absolute values of the causal effects themselves, for which no independent data exist against which such a comparison could be made. Internal consistency is nonetheless a meaningful evaluation, since the absolute values of the causal effects depend on a wide variety of factors that are not always attributable to the real-world system alone, but also to the capacity of the random forest estimator to resolve the effects of individual variables. We therefore focus on the dispersion of the results within individual basins as an indicator of estimation stability. A low coefficient of variation after trend correction indicates that the residual variability around the estimated trend is small relative to the mean, which we interpret as evidence that the method produces consistent rather than erratic results. For each basin, we calculate the coefficient of variation (CV) as well as a trend corrected version of it (Trend-CV) using the Theil-Sen slopes described in Sect. 3.2. The CV is defined as:

$$\mathrm{CV} = \frac{\sigma}{\mu} \tag{1}$$

where σ is the standard deviation and μ is the mean of the dataset.

The Trend-CV respectively is calculated as follows:

$$\text{Trend-CV} = \frac{\sigma_{\text{residual}}}{\mu_{\text{residual}}} \tag{2}$$

Here, σ_{residual} is the standard deviation of the residuals, and μ_{residual} is the mean of the residuals, defined as:

$$\text{residual} = y_i - \hat{y}_i \tag{3}$$

where y_i is the actual value and $\hat{y}_i$ is the predicted value. CV and Trend-CV were calculated for the full time series of snowmelt and rain causal effects on river discharge, as well as for a truncated time series (1985–2017). This truncation is necessary because the moving window approach used in the method leads to smaller sample sizes at the beginning and end of the time series, compared to the center. A Wilcoxon signed-rank test reveals that a significant portion of the dispersion arises from these time series ends. Furthermore, comparing the CV with the Trend-CV indicates that the trend itself accounts for a substantial part of the observed dispersion. This pattern also holds for the Trend-CV, where the ends of the time series contribute markedly to the overall variability. A summary of the dispersion metrics is shown in Fig. 13.

4 Discussion

4.1 Contextualization of Results

4.1.1 Global and Large-Scale Studies

As mentioned in the Sects. 2 and 3.5, no adequate and independent validation data are currently available to validate the causal effect trends in this paper. While our sanity tests with modified trigger variables demonstrated that the method adequately captures such changes, this only validates its internal functionality and does not confirm the accuracy of the actual effects. Therefore, the study should be viewed as an experimental data analysis to test the applicability of the presented methods. Nevertheless, we aimed to contextualize our results with already published studies. Accordingly, we incorporated global studies from a review (Schilling et al., 2024) and conducted a systematic literature search via Web of Science (WOS), using various terms concerning SWE, streamflow and driving factors, subsequently evaluating their relevance to our findings. Given the use of partly identical data, the global trends align with those already published at the global level, as expected. While differences in aggregation and representation might result in differing interpretations, the trends presented here are consistent with what is to be expected and fall within the anticipated range (TWS; Zhang et al., 2019, river discharge: Shi et al., 2019; Park et al., 2024, SWE; Pulliainen et al., 2020, precipitation; Sun et al., 2021, SM; Mohseni et al., 2023, groundwater (baseflow flux); Hasan et al., 2023, temperature: Wang et al., 2022, evapotranspiration Li et al., 2023).

When the scope is expanded to river-discharge contribution as well as flood-generating studies, several studies align with the general mechanisms and snow dominance depicted in our analysis (Do et al., 2020; Zhang et al., 2023; Robinson and Clark, 2020) on a global level, or on continental (Europe; Jiang et al., 2022; Fang et al., 2024, North America; Li et al., 2019) and Arctic scale Park et al., 2024). These studies confirm the trends described in Sect. 1.1, towards earlier and faster snowmelt periods. Examining the exemplary basins shows that the Colorado and Indus basins are well represented in the literature, the Danube, Po, and Mackenzie basins have somewhat lower coverage, and the Yenisey basin shows very limited documentation based on English-language publications. In terms of content, the smaller-scale studies confirm the global trends, and certain regional patterns emerge.

4.1.2 Basin-specific patterns

In the Danube and Po basins, which both have their headwaters in the Alps, the discharge in the entire basin is dependent on the corresponding snowpack, especially in drought years (Chen et al., 2020; Stagl and Hattermann, 2015; Guastini et al., 2019; Coppola et al., 2014; Vezzoli et al., 2015; Avanzi et al., 2024). For rain, the two basins developed in opposite directions: the causal effect of rain on river discharge increased significantly in the Po, alongside a significant increase in both the rainfall anomaly and the coupling strength of discharge to rain, whereas in the Danube it decreased, despite a significant increase in the rainfall anomaly there as well, while the coupling strength of discharge to rain showed a non-significant decrease. For snowmelt, both

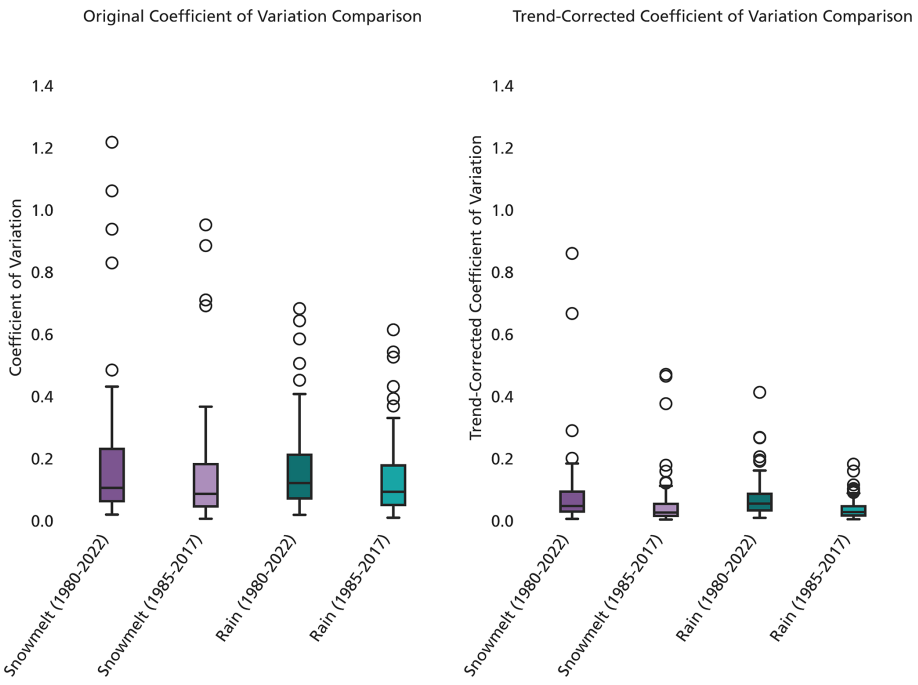


Figure 13. Measures of Dispersion for causal effect on river discharge trends of both snowmelt and rain over all basins. Left: coefficient of variation. Right: Normalized RMSE, corrected for the Theil-Sen trend displayed in Sect. 3.2.

basins showed a non-significant positive trend in the causal effect, alongside a non-significant increase in the snowmelt anomaly and a non-significant decrease in the coupling strength of discharge to snowmelt in both cases. In the Po, the combined growth of the rainfall anomaly and an increased coupling between rain and discharge indicate that a larger fraction of precipitation is transformed into discharge directly, in a strongly snow-dominated and comparatively small basin. This is consistent with the higher contribution of snowmelt to total discharge in the Po compared to the Danube, where rainfall accounts for a larger share of the annual water balance (Stagl and Hattermann, 2015; Vyshnevskyi and Shevchuk, 2022; Formetta et al., 2022). In the Danube, by contrast, the growing rainfall anomaly is not matched by a strengthening coupling, and instead the causal effect of rain on discharge weakens. This would be consistent with a more buffered flow regime, in which soil moisture, groundwater and human regulation increasingly decouple precipitation inputs from immediate river discharge, though as neither the coupling strength trend nor the snowmelt trends in either basin reach statistical significance beyond the rainfall anomaly itself, we refrain from a stronger mechanistic interpretation of these patterns. Additional factors such as topography, river regulation and urbanization may further shape basin-specific responses but cannot be resolved without more detailed local analyses. In both basins, glaciers currently help to stabilize discharge as long as they continue to melt at approximately present rates (Van Tiel et al., 2021; Lambrecht and Mayer, 2024; Penna et al., 2017; Huss, 2011), which is consistent with global evidence for a stabilizing role of glacier melt under warming conditions (Ultee et al., 2022).

The Colorado basin shows similar characteristics with the Po and Danube basins, with headwaters in mountains flowing into a plain with limited snowfall. However, the plains in the Colorado basin are more arid than in the European examples, which imparts its specific characteristics to the basin. Therefore, the basin is very dependent on its seasonal snowpack (Webb et al., 2024), but as it is drier than the Po and Danube, the amount of summer precipitation seems to have a more crucial impact on the overall hydrological balance (Flynn et al., 2024; Ban et al., 2023). This is also supported by Wolf et al. (2023), who states that groundwater is a crucial streamflow driver during late summer and autumn. Additionally the soil moisture seems to play a not fully understood role in the Colorado basin, for example, Talsma et al. (2022) have observed strongly erratic behavior of soil moisture data in the Colorado Basin (as also seen in our findings), and Julander and Clayton (2018) found for small basins in Utah that above-average rainfall does not drive runoff proportionally. Also it is to consider that other storage mechanisms such as soil moisture and groundwater become more crucial, which complies with the findings of Wolf et al. (2023) as well as Julander and Clayton (2018), even though they are declining (see Fig. 7). Overall this paints a picture of a basin that experiences increasingly dry conditions, and has to rely more and more on single weather events to recharge its storage, as the general storage level has decreased in the last years. The coupling strength of dis-

charge to snowmelt decreased significantly, and the coupling strength of discharge to rain decreased as well, despite significant increases in both the snowmelt and rainfall anomalies, indicating that rain and snowmelt are translated into runoff less efficiently than before. This decline in hydrological effectiveness has been demonstrated in recent years. Even record-high snowpack in 2023 failed to adequately recharge groundwater reserves or generate proportional streamflow increases (Carroll et al., 2024). Recent isotope studies show that during peak snowmelt, streamflow is increasingly dominated by aged groundwater rather than direct snowmelt contributions, indicating that precipitation is increasingly delayed and decoupled from immediate runoff (Brooks et al., 2025). Taken together, earlier and faster snowmelt driven by warming temperatures compresses the melt period and reduces water availability during critical late-summer low-flow periods. Similarly, summer rainfall becomes increasingly decoupled from runoff generation, potentially due to increased evapotranspiration or limited soil infiltration capacity under water stress. Despite this declining efficiency, the causal effect of rain on river discharge showed a significant positive trend, and the causal effect of snowmelt a non-significant positive trend, driven primarily by the growing magnitude of the underlying anomalies rather than by a strengthening coupling between the trigger variables and discharge. The Colorado thus faces a dual challenge: declining water availability combined with a reduced efficiency in translating the water that does arrive into streamflow, even as increasingly extreme deficit years leave a growing mark on the causal footprint of both snowmelt and rain, a pattern that underscores the basin's heightened vulnerability to further climate change.

In the Arctic, the Mackenzie, but not the Yenisey, aligns with the general Arctic trend of increased discharge (Park et al., 2024), however in the Mackenzie the discharge trend is basically flat, while it is significantly decreasing in the Yenisey. Generally and comparable to the Alpine basins, these basins see faster and shorter melt periods (Yang et al., 2021; Mavromatis et al., 2016). Also several regional dynamics seem to apply, for instance Krogh and Pomeroy (2018) showed that a series of snow-hydrological processes in a small subbasin of the Mackenzie are slowing down, and sublimation and evapotranspiration have dropped, mitigating the reduced precipitation in the subbasin. The latter is not true for the entire basin, but could indicate changing dynamics within the basin, in which, alongside decreasing soil moisture and baseflow flux trends, snow as a storage component leaves a growing mark on river discharge, consistent with the positive causal effect trend we find for snowmelt in the Mackenzie. However, the underlying coupling strength of discharge to snowmelt decreased significantly in the Mackenzie, in contrast to the Yenisey, where the causal effect of snowmelt on discharge increased significantly, alongside a non-significant increase in both the snowmelt anomaly and the coupling strength of discharge to snowmelt. For the Yenisey, Zakharova et al. (2011) shows that over time, less snowmelt was ending up as river discharge in the region due to increased evaporation and sublimation. Also Gordeev et al. (2024) suggests that a decreasing influence of bogs could cause an observed increasing role of Al-rich colloids and subcolloids. These results suggest that rising temperatures increase sublimation, and the correspondingly thawing permafrost allows for greater water infiltration into the ground (Kurylyk and Walvoord, 2021), which would be expected to weaken, rather than strengthen, the direct coupling between snowmelt and discharge. Our finding of a slightly increasing coupling strength in the Yenisey does not straightforwardly align with this mechanism. It may instead reflect that reduced precipitation (both snow and rain) leads to lower soil moisture and groundwater recharge, making the storage function of SWE increasingly important as a more direct source of streamflow once other pathways are depleted. Therefore, although local research indicates increased infiltration of precipitation into the ground and delayed river flow, our results suggest that the growing magnitude of the snowmelt anomaly, and possibly this compensating storage effect, together outweigh any weakening of the snowmelt-discharge coupling in terms of the resulting causal effect on streamflow generation. These dynamics could also apply for the Mackenzie basin, where permafrost is also thawing (Kurylyk and Walvoord, 2021), and apart from the river discharge and rain trend all other variable trends develop in the same direction as the trends in the Yenisey. Unlike the Yenisey, however, the coupling strength of discharge to snowmelt in the Mackenzie decreased significantly rather than increasing, suggesting that the two basins, despite comparable permafrost dynamics, differ in how effectively snowmelt anomalies are converted into discharge.

Since climate in the Indus basin is mostly dominated by the Westerlies instead of Monsoon seasons, as it is in other Himalayan basins, the Indus basin shares various similarities with other basins in this analysis. It has snow-rich, strongly glacierized mountains in the headwaters, and arid regions downstream. However, the Indus stands apart from Colorado, Danube, and Po, since its glacier mass surpasses the others by magnitudes. Therefore the main driver in streamflow generation is the glacier melt (Immerzeel et al., 2010; Bolch et al., 2012; Yao et al., 2022) and snowmelt seems to only play a secondary role (Kumar et al., 2024; Soheb et al., 2024; Joshi et al., 2023; Shafeeque et al., 2023). Glacier melt has been increasing during our study period, though it is believed that peak water has not yet been reached (Lutz et al., 2014; Pritchard, 2019; Huss and Hock, 2018). The coupling strength of discharge to snowmelt increased significantly in the Indus basin, while the coupling strength of discharge to rain decreased significantly. Both the causal effect of snowmelt and of rain on river discharge showed a positive, non-significant trend, coinciding with a non-significant increase in the snowmelt anomaly and a significant increase in the rainfall anomaly. Since the Indus basin is highly glacierized, glaciers play a major role in streamflow generation,

and summer rainfall often coincides with peak glacier melt, when meltwater already dominates streamflow. This temporal overlap might explain the decreasing coupling strength of discharge to rain, as rainfall's marginal contribution is increasingly masked by the glacier melt signal during the main runoff season (Lutz et al., 2014; Bolch et al., 2012; Pritchard, 2019; Immerzeel et al., 2010). The increasing coupling strength of discharge to snowmelt, by contrast, corresponds to increased winter precipitation, which typically occurs before the main glacier melt season; during this period, the snow cover also protects the glacier surface from direct exposure (Lutz et al., 2014; Pritchard, 2019), delaying melt onset and stabilizing runoff, consistent with a strengthening direct coupling between snowmelt and discharge. However, our finding of an increased causal impact of snowmelt on river discharge is partially contradictory to the findings of Adnan et al. (2022), Ali et al. (2023), Adnan et al. (2024), and Chandel and Ghosh (2021), which however all were conducted in the mountainous parts of the basin. It is also to note that Immerzeel et al. (2015) found that precipitation in high altitudes in the Himalayas is systematically underestimated in most models or gridded precipitation products. Furthermore there is also evidence, that the earlier snowmelt influences the spring runoff in the Indus basin, which in turn supports our findings of an increased causal impact of snowmelt on river discharge (Wang et al., 2025; Hasson et al., 2017; Sharif et al., 2013; Guo et al., 2025). Therefore, our findings can be reasonably aligned with existing literature. Given indications of earlier snowmelt onset and an overall increase in snowfall, it appears possible that snowmelt has become relatively more important for basin-wide streamflow generation, although its overall role likely remains secondary to glacier melt.

4.1.3 Cross-basin synthesis and broader implications

Across the six exemplary basins, the magnitude of the snowmelt anomaly increased in all cases, though only significantly in the Colorado, while the resulting coupling strength of discharge to snowmelt diverged by basin type: it decreased in the Mackenzie, Colorado, Danube, and Po, the basins with mountain headwaters feeding arid or temperate lowlands (significantly in the Mackenzie and Colorado), while it increased in the Yenisey and the Indus, the two basins most strongly impacted by permafrost and by extensive glaciation, respectively (significantly in the Indus). For rain, the coupling strength of discharge decreased in five of the six basins (significantly in the Mackenzie and the Indus), with the Po as the sole exception, where it increased significantly alongside a significant increase in the rainfall anomaly. This indicates that the increasing causal role of snowmelt and rain observed across most exemplary basins is, in the majority of cases, driven primarily by growing anomalies in the trigger variables themselves rather than by a systematically strengthening coupling between these variables and discharge. A stronger direct coupling coincides with the anomaly increase in the most strongly cryosphere-dominated of the exemplary basins for snowmelt, and in the Po for rain.

Finally, we can conclude that our results support the qualitative examination for the exemplary basins and align well with the current state of research. However, it is important to acknowledge that studies verifying the relative influence of snowmelt on river discharge, particularly at our spatial and temporal scales, remain scarce. As a result, our qualitative analysis relies more on indicative findings and approximations than on direct empirical evidence. It is worth noting that although our primary focus is on snowmelt and rain, glacier melt plays a crucial role in certain hydrological systems. We included glacier melt in our analysis to account for its presence, but we did not compute its causal effects. Therefore, glacier melt remains a source of uncertainty when explaining the causal effects of snowmelt and rain. This uncertainty may influence the interpretation of results in basins where glaciers are present. A similar challenge applies to human influences. Currently, there is no comprehensive global dataset quantifying human impacts on hydrological regimes. For this reason, we chose not to include human influences in our setup, even though they can have a considerable effect on certain variables. For example, irrigation in agriculture appears to alter groundwater signals and seasonality in some regions (Carlson et al., 2025; Hall et al., 2024). Similarly, thawing permafrost dynamics remain a major source of uncertainty in especially arctic regions Wang et al. (2021). Despite these complexities in the explainability of our findings, our results focusing on snowmelt and rain remain valuable, especially given the prevailing consensus that declining snow water equivalent trends in the Northern Hemisphere lead to faster and earlier melt. These changes, combined with more erratic precipitation patterns and prolonged drought periods, make snow increasingly important as a water storage resource. This is particularly relevant in 38 basins where our method detected an increasing trend in the causal effect of snowmelt on river discharge, even though both snow water equivalent and river discharge showed declining trends. Such regions warrant special attention from researchers and policymakers alike, as regional water availability appears increasingly dependent on snow as a diminishing resource.

Our research also shows that the causal effect of snowmelt on river discharge, as examined in this study, can add a new relative dimension to snow hydrology, which is linked, but not the same, as sole snow dominance. Therefore, snow dominance can decline in a certain region, while the causal effect, and thus the relative impact is increasing, as it quantifies the influence of snowmelt on river discharge as is carried out trough the overall system. For a deeper understanding of the dynamics in a basin, these two measures should therefore be considered together. Moreover, the decomposition into anomaly magnitude and coupling strength presented here adds a further layer to this relative dimension: an increasing causal effect does not necessarily indicate that

a system responds more strongly to snowmelt or rain, but may instead reflect that the underlying anomalies themselves have grown. Distinguishing between these two possibilities is relevant for anticipating how basins may respond to further changes in snowmelt and rainfall variability. The qualitative analysis also shows that the method developed here can be applied in various hydrological regimes and climates, and thus can support hydrological studies in a wide range of basins.

4.2 Methodological Discussion

The general intention of this study was to design a causal inference setup capable of capturing the dynamics between snowmelt and river discharge across various regions and extended time periods, enabling comparisons across these spatial and temporal scales. This became necessary as our literature revealed a lack of large-scale studies in the intersection of snow, SWE, and river discharge, using advanced analytical methods. Therefore, all decisions concerning the study design, served the purpose of setting up a resilient and widely applicable method, rather than providing a precise depiction of various local conditions across the study region. Accordingly, the methodological set-up comprises multiple considerations which reflect this optimization towards a broad framework, rather than local accuracy.

Firstly, the selection of data was constrained by spatial and temporal requirements, and while all incorporated datasets are validated and peer-reviewed, they each carry inherent strengths, limitations, and uncertainties. Some datasets also required preprocessing to align with the time-series requirements of PCMCI+, involving several assumptions that, while necessary and well-supported by literature, may have affected local accuracy. Furthermore, the data were spatially and temporally aggregated, which affects the ability to capture small scale variations in the data, both spatial and temporal. However, these aggregations were necessary to balance the representation of large spatial and temporal scales with the need for an expedient time lag within the causal inference framework, while minimizing computational demands. Moreover, depicting hydrological context within a scientific approximation is a complex task, which by itself normally already includes various simplifications and assumptions, based on the current knowledge of the topic. For our study, this meant that not all relevant processes could be incorporated in the system, which is additionally limited by the informative capability of the utilized datasets. However, by focusing on the land surface dynamics of the systems, leaving out all atmospheric processes and land-atmosphere interactions, we could include the key variables for streamflow generation in the studied river basins. Nonetheless, LPCMCI can be considered as an alternative to PCMCI+ for accounting for additional, potentially hidden variables influencing the estimated causal effects. During our development process, we tested the LPCMCI in multiple set-ups, which however did not yield realistic causal effects. One key decision, where we opted to represent local conditions as well as possible was the selection of the intervention in the causal effect estimation. By intervening the system seasonally and per basin, we adequately depict each basin's conditions, even though the intervention values are still averaged over the full basin, thus potentially losing more small scale details. The intervention choice ($\mathrm{do}(X = \mu)$ vs. $\mathrm{do}(X = \mu - \sigma)$) was furthermore driven by the research question regarding the sensitivity of river discharge to a typical anomaly in snowmelt and rain, rather than their total contribution. This choice, however, introduces a further limitation to consider when comparing causal effects across variables and basins: since σ is estimated separately for each variable, season, and basin, the magnitude of the intervention itself varies accordingly. A low causal effect can therefore either indicate a genuinely weak coupling between the trigger variable and discharge, or simply reflect a comparatively small typical anomaly (σ) of the trigger variable in that basin, rather than a weak underlying sensitivity of discharge to it. Consequently, absolute causal effect magnitudes should not be directly compared between variables (e.g. snowmelt vs. rain) or between basins without considering the underlying variability of the respective trigger variable.

Besides the various decisions towards better comparability over the depiction of local mechanisms, the development process was also characterized by the balance between enabling PCMCI+ to detect effects, and managing the computational demand. The causal inference requires a certain data sample to reliably detect causal effects for a system (Kathpalia et al., 2022), therefore the sample used to calculate the causal effects needed to be chosen adequately, but in a fashion that within the moving window approach, the computational demand lies within the possibilities of our available infrastructure. The moving window approach itself, which was superimposed on to the causal inference framework, adds certain challenges, mainly concerning the yearly averaging, the years on the temporal edges of the time-series are underrepresented, and are thus susceptible to outliers. As most of the calculated averages used for the trend derivation rely on a broad sample, we refrained from clipping the time-series or introducing shorter additional windows at the edges of the time-series. However, this is one reason why we present trends and not absolute values in this study. Another reason is because absolute values of causal effects are generally dependent on how well the methodical setup recognizes them within the data, which might not always represent the reality. Another sign pointing to this circumstance is that for rain, the link between trigger and target variable was found more often than for snowmelt. This reflects a difference in effective sample size between the two signals rather than a shortcoming of the causal inference framework itself: rain occurs throughout the year and yields up to 26 biweekly data points per year, whereas snowmelt occurs only during a limited period of the year, yielding approximately 4–8 biweekly

data points per year per basin. This smaller effective sample size reduces the statistical power to detect causal links for snowmelt compared to rain. As this limitation arises from the physical nature of the variables themselves, any causal inference method informed by the data would face the same constraint. We note that where PCMCI+ does not detect a link for a given basin and period, the causal effect estimation returns zero. This may in part reflect the limited effective sample size of the snowmelt signal rather than a genuine absence of a causal relationship.

The presented results are all a ratio of the causal effect to the mean discharge in a certain basin, thus showing a relative change within a basin, which is less dependent on the ability of recognition within the data by PCMCI. Within basins the analyzed performance metrics (see Sect. 3.5) show that the yearly values fluctuate on an acceptable level, and the trend derivation thus can be regarded as robust. Also by fitting Theil-Sen slopes we additionally mitigate against any kind of fluctuation within the results, adding to the resilience of the trend statements.

Nevertheless, despite the Theil-Sen method being more robust concerning outliers, it is still a linear fitting method, and thus only remains valid under the assumption of a linear trend. Therefore, for causal and variable trends, we classified the trends by the sign of the slope regardless of the gradient. This was necessary to enable a comprehensive comparison of the method among the basins, and a possibility to categorize them. It, however, might suggest that conditions in a basin are more severe or extreme, than they are if one considers the actual data. It, however, also became an inevitable step, to avoid a multitude of potential additional categorizations, which would complicate an expedient comparison. However, it also underscores the need for a thorough analysis of basin-specific data, as exemplified in Sect. 3.4 for select basins, to inform qualified statements about the unique circumstances within a given basin.

Generally, as shown in the analysis of exemplary basins in Sect. 3.4, the estimation of causal effect serves as a valuable measure for understanding hydrological dynamics that cannot be captured by individual variables alone. The causal effect can support the determination of certain dynamics and narrowing down unknown developments. However, PCMCI+ is run per basin, and thus referenced to the corresponding basin discharge, which limits the comparability among basins generally. Because of this, but also given the complexities in detecting effects based on sample size, we recommend using the causal effects computed in this study only to assess relative changes, and as a complementary rather than standalone measure when examining snow-hydrological systems in a given study region.

The use of trends as indication of relative change is additionally supported by the statistical metrics presented in Sect. 3.5. The analysis of the dispersion of the calculated causal effects shows that significant portions of the dispersion are due to the trend itself and the small sample size at the ends of the time series. For a predominant majority of the basins, the trend-corrected dispersion falls within a suitable range for this analysis. Considering that with the Theil-Sen estimator, we used a fitting method which is robust against outliers, we regard the use of trends and thus relative changes as justified.

To conclude, we acknowledge the simplifications and compromises inherent in our study. Our results must be interpreted within the context of individual basins, regional climate dynamics, and broader continental influences. It should be noted that, with the current setup, the results reflect the method's ability to identify causal structures in the data, which may not always translate directly into absolute real world effect magnitudes. Nonetheless, this study introduces a novel, data-driven approach to snow-hydrology that extends beyond conventional statistical measures and small-scale applications. The method has demonstrated adequate responses in plausibility tests and, while still experimental, provides a foundation for future research, both methodologically and in more localized contexts. Despite the challenges of estimating causal effects in snow-hydrology, our findings demonstrate the potential of this approach to complement established methodologies and advance the understanding of hydrological systems.

5 Conclusions

Snowmelt is a crucial contributor to river discharge in various regions on the Northern Hemisphere. It sustains over 1.5 billion people as a societal water supplier, supports key industries like agriculture and hydropower, and impacts regional ecosystems. Due to climate change, snow water equivalent (SWE) is declining, reducing snow-based water availability. A review of large-scale SWE studies reveals that the relationship between SWE and river discharge has rarely been examined beyond basic statistical measures, which cannot capture the complexity of hydrological regimes. To address this gap, we developed a causal inference approach based on Peter and Clark Momentary Conditional Independence Plus (PCMCI+). PCMCI+ performs causal discovery and detects a network of causal links within a multivariate system. PCMCI+ is followed by a causal effect estimation which quantifies the effect of a trigger variable onto a target variable within the same system. Our system includes river discharge, snowmelt (defined as SWE depletion), rain, glacier runoff, baseflow flux, soil moisture, evapotranspiration, temperature, and the date as a deterministic time variable, with lags of up to six months. Causal effects of snowmelt and rain on river discharge were estimated applying a moving 20-year window to the 1980–2022 time series. The resulting effects were summed and then divided by the period's mean river discharge and finally averaged by year. The yearly averages were used to quantify trends with a Theil-Sen estimator. We present these causal effect trends for 119 Northern Hemisphere basins, alongside Theil-Sen trends for individual

variables. In addition, we examine six representative basins to illustrate differing hydrological and geographic dynamics. Based on these results, several overarching conclusions can be drawn:

- Our trend analysis confirmed a decreasing trend for SWE in a majority of the examined basins (94/119).
- Also, the trends for river discharge (79/119) and rain (71/119) in the catchments are predominantly negative.
- Looking at patterns among these discharge, rain, and SWE trends, two major dynamics become apparent. Firstly, in all Arctic basins (except Yenisey) the SWE trend is negative while the rain trend is positive. Secondly in lower latitudes, the basins where all these trends are negative make up the largest share of the basins (51/102).
- Of all basins where a causal effect for snowmelt on river discharge was detected, 64 of 73 (88 %) showed an increasing trend. For the causal effect of rain on river discharge 97 of 114 (85 %) had an increasing trend.
- For the causal effect of snowmelt on river discharge, the largest increasing trend was found in the Columbia basin (USA/Canada), the steepest decrease was found in the Ziya He Interior basin in China.
- Correspondingly the largest increasing trend was seen in the Baltic Sea East Coast, the steepest decreasing trend in the Lena basin (Russia).
- No effects could be found using correlation of the causal effect trends against latitude, mountainous portion of the basin, or snow dominance.
- In 40 basins, our method detected an increasing causal effect of snowmelt on river discharge, despite declining trends in SWE and river discharge. These areas are critical for researchers and policymakers, as they indicate water availability is increasingly reliant on snow, despite it being a diminishing resource. This can have various implications for funding decisions in water management, conservation, and research.
- For the six exemplary basins (Mackenzie, Colorado, Danube, Po, Yenisey, and Indus), decomposing the causal effect trends into anomaly magnitude and coupling strength revealed a consistent pattern among the four basins with mountain headwaters feeding arid or temperate lowlands (Mackenzie, Colorado, Danube, Po): in all four, the coupling strength between snowmelt and discharge decreased despite a growing snowmelt anomaly. The Yenisey and the Indus, in contrast, are shaped most strongly by permafrost and extensive glaciation, respectively, and both showed an increasing coupling strength for snowmelt. For rain, coupling strength decreased in five of the six basins, with the Danube as the sole exception.
- The causal effect of snowmelt on river discharge can increase despite decreasing SWE trends, and even despite increasing trends in rain and in the causal effect of rain on river discharge. Decomposing the causal effect trend indicates that, across most basins, this increase is primarily driven by a growing magnitude of the snowmelt anomaly itself, rather than by an increased coupling between snowmelt and discharge.
- Dispersion metrics (Coefficient of Variation; CV, and trend-corrected CV, Trend-CV) show that generally our method is suited for trend derivation, especially as a significant portion of the dispersion is due to the ends of the time series and their reduced sample size in the moving window approach, as well as the trend itself.

Although our method did not detect causal effects, and therefore trends, in all basins, and the effect size depends on the selected random forest estimator, it advances large-scale snow hydrology by capturing the complexity of hydrological regimes beyond conventional statistical approaches. To enable large-scale comparison, we made several methodological decisions that prioritized comparability over local accuracy. While this allowed for the analysis presented in this study, it limits the resolution of local dynamics within basins. Despite these limitations, we demonstrated that causal effects, even within an experimental framework, are a suitable means of assessing relative changes in the importance of snowmelt, which does not necessarily align with snow dominance itself. Within this experimental framework, causal inference can add an additional layer to existing hydrological analyses, with further methodological refinements potentially expanding its applicability in future research.

Appendix A: Hydrological System for Causal Discovery

Figure A1 expands on the hydrological links described in Sect. 2.5.1. These links reflect established hydrological and atmospheric relationships and constrain the search space of PCMCI+ without imposing fixed causal connections. For example, the evapotranspiration variable used in this study intentionally excludes open-water evaporation, which operates directly at the river surface rather than through terrestrial pathways, and snow sublimation, whose inclusion would contradict the snowmelt definition used in this study (Sect. 2.3.1). Within this definition, evapotranspiration influences river discharge only indirectly, through soil moisture depletion, which is explicitly included as a mediating variable in the causal graph; no direct link from evapotranspiration to river discharge is therefore specified.

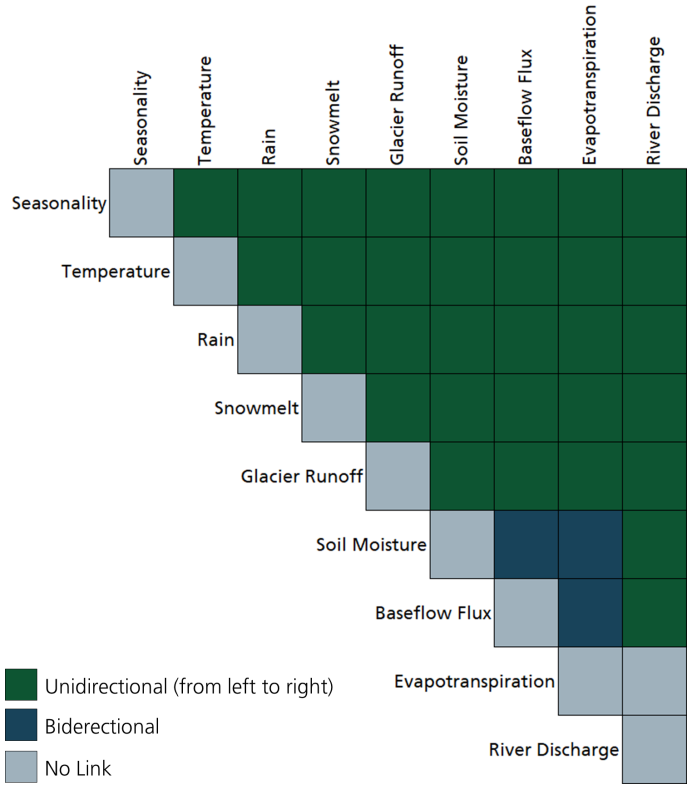


Figure A1. The assumed potential links between the variables used in the causal discovery phase. Evapotranspiration is linked to river discharge only indirectly via soil moisture; open-water evaporation and snow sublimation are excluded from the evapotranspiration definition.

Appendix B: Full Results

This appendix provides the complete results shown as maps in Sect. 3, presented here as tables with corresponding colors. The figures are grouped by continent.

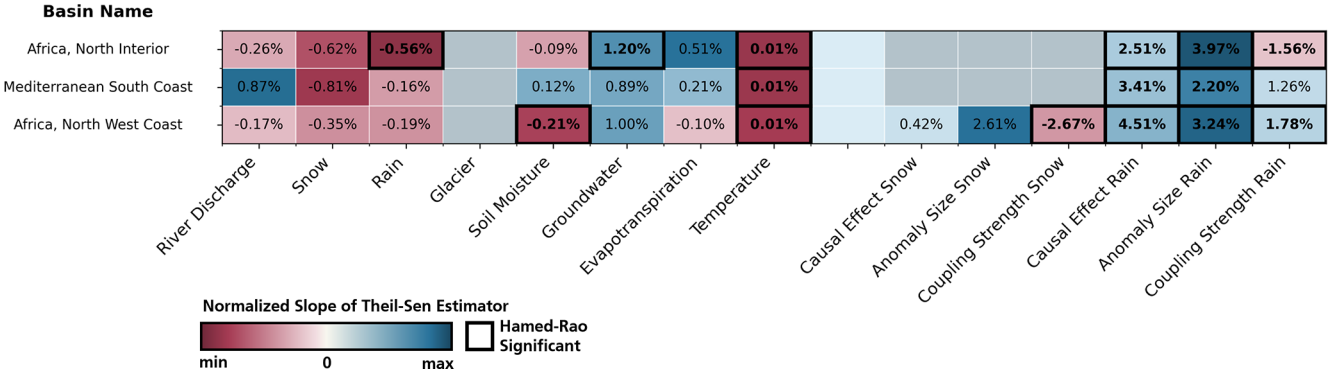


Figure B1. Relative variable trend slopes for all African basins normalized with the basin mean per variable (left) and causal effect trend slopes as absolute values (ratio of causal effect to mean discharge) as well as relative values, normalized with the basin mean (right). The colorscale for the temperature is inverted.

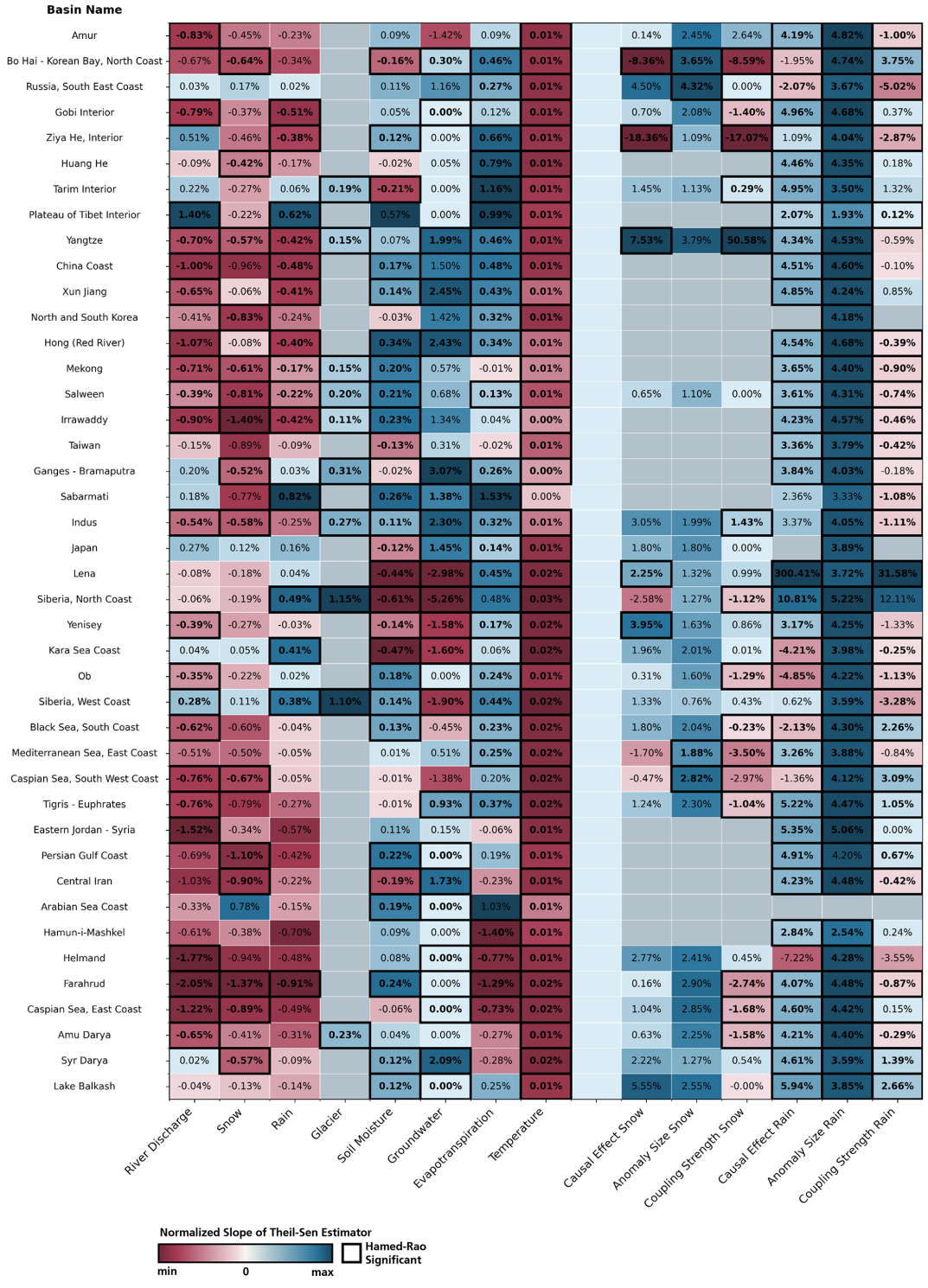


Figure B2. Relative variable trend slopes for all Asian basins normalized with the basin mean per variable (left) and causal effect trend slopes as absolute values (ratio of causal effect to mean discharge) as well as relative values, normalized with the basin mean (right). The colorscale for the temperature is inverted.

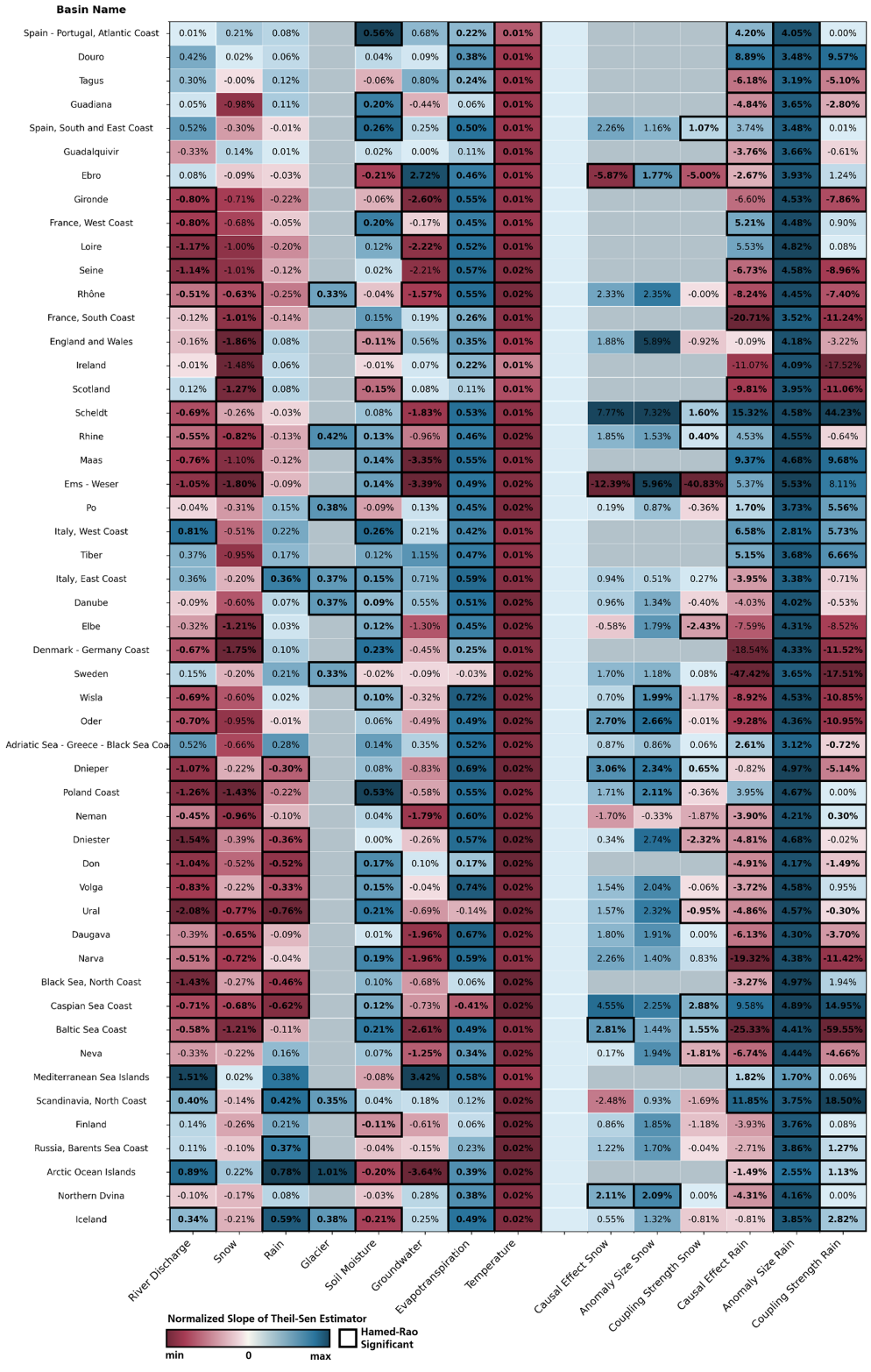


Figure B3. Relative variable trend slopes for all European basins normalized with the basin mean per variable (left) and causal effect trend slopes as absolute values (ratio of causal effect to mean discharge) as well as relative values, normalized with the basin mean (right). The colorscale for the temperature is inverted.

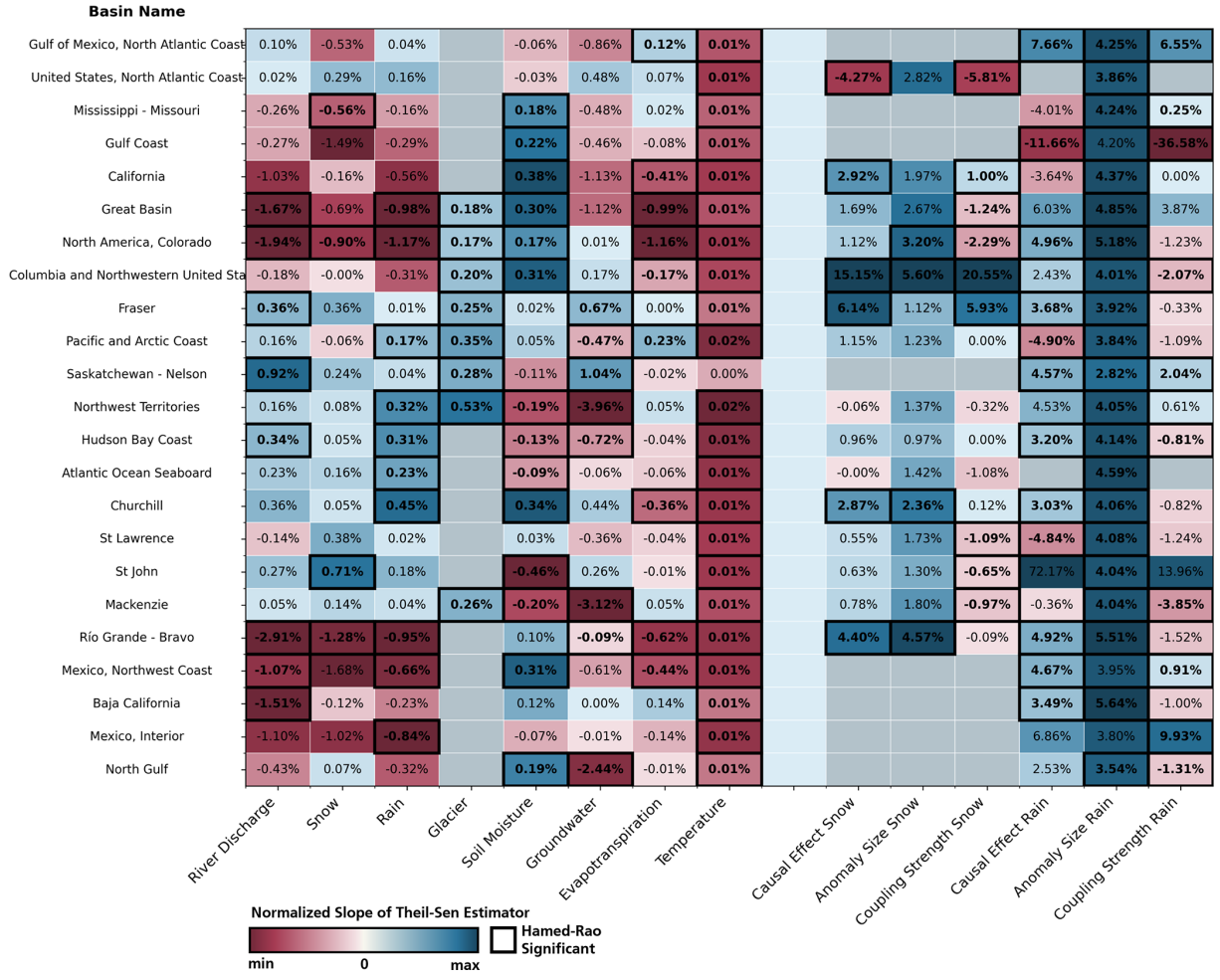


Figure B4. Relative variable trend slopes for all North American basins normalized with the basin mean per variable (left) and causal effect trend slopes as absolute values (ratio of causal effect to mean discharge) as well as relative values, normalized with the basin mean (right). The colorscale for the temperature is inverted.

Code availability. The analysis code used in this study is available on request from the corresponding author.

Data availability. All datasets used in this study are publicly available. They are described in Sect. 2.2 and listed in Table 1. Their preprocessing is described in Sect. 2.3, and all of them are used in the analyses in Sect. 2.4 and 2.5. The datasets and their sources are: basin outlines from FAO (FAO, 2011), rain from ERA5 (Hersbach et al., 2023), temperature and snow water equivalent from ERA5-Land (Muñoz Sabater, 2019), river discharge from GloFAS v4.0 (Grimaldi et al., 2022), soil moisture from ESA CCI (Dorigo et al., 2019), baseflow flux and glacier runoff from MERRA-2 (GMAO, 2015a, b) and evapotranspiration from GLEAM v4.1 (Miralles et al., 2025). Dataset-specific preprocessing steps are described in Sect. 2.3.1 (snow water equivalent and snowmelt), Sect. 2.3.2 (rain) and Sect. 2.3.3 (glacier runoff). The persistent identifiers (DOIs) are given in the corresponding reference list entries.

Author contributions. Initial conceptualization, S.S., A.D. and C.K.; Causal inference setup S.S. and R.J.H.; hydrological setup and contextualization S.S. and T.B.; writing – original draft preparation, S.S.; writing – review and editing, all authors; visualization, S.S.; supervision, C.K. All authors have read and agreed to the published version of the manuscript.

Competing interests. At least one of the (co-)authors is a member of the editorial board of *The Cryosphere*. The peer-review process was guided by an independent editor, and the authors also have no other competing interests to declare.

Disclaimer. Publisher's note: Copernicus Publications remains neutral with regard to jurisdictional claims made in the text, published maps, institutional affiliations, or any other geographical representation in this paper. The authors bear the ultimate responsibility for providing appropriate place names. Views expressed in the

text are those of the authors and do not necessarily reflect the views of the publisher.

Acknowledgements. We would like to thank Prof. Dr. John Pomeroy for his initial consultation on hydrological systems in the Northern Hemisphere. Furthermore we would like to express our gratitude to Sanju Sajimon for his support in various parts of the literature research.

The work and publication of this study were supported by the DLR internal EO4AlpineRisks project.

Rebecca Jean Herman has received funding from the European Research Council (ERC) Starting Grant CausalEarth under the European Union's Horizon 2020 research and innovation program (grant agreement No. 948112).

Large Language Models were used to support code development in this study and to refine the language of this publication.

Review statement. This paper was edited by Carrie Vuyovich and reviewed by Alexander Gottlieb, Haejo Kim, and Samuel Tuttle.

References

Adnan, M., Liu, S., Saifullah, M., Iqbal, M., Ali, A. F., and Mukhtar, M. A.: Spatiotemporal variations in runoff and runoff components in response to climate change in a glacierized subbasin of the Upper Indus Basin, Pakistan, Front. Earth Sci., 10, 970349, https://doi.org/10.3389/feart.2022.970349, 2022.

Adnan, M., Liu, S., Saifullah, M., Iqbal, M., Saddique, Q., Ul Hussan, W., and Latif, Y.: Estimation of changes in runoff and its sources in response to future climate change in a critical zone of the Karakoram mountainous region, Pakistan in the near and far future, Geomatics, Nat. Hazard. Risk, 15, 2291330, https://doi.org/10.1080/19475705.2023.2291330, 2024.

Ali, Z., Iqbal, M., Khan, I. U., Masood, M. U., Umer, M., Lodhi, M. U. K., and Tariq, M. A. U. R.: Hydrological response under CMIP6 climate projection in Astore River Basin, Pakistan, J. Mountain Sci., 20, 2263–2281, https://doi.org/10.1007/s11629-022-7872-x, 2023.

Avanzi, F., Munerol, F., Milelli, M., Gabellani, S., Massari, C., Girotto, M., Cremonese, E., Galvagno, M., Bruno, G., Morra di Cella, U., Rossi, L., Altamura, M., and Ferraris, L.: Winter snow deficit was a harbinger of summer 2022 socio-hydrologic drought in the Po Basin, Italy, Commun. Earth Environ., 5, 1–12, https://doi.org/10.1038/s43247-024-01222-z, 2024.

Ban, Z., Li, D., and Lettenmaier, D. P.: The Increasing Role of Seasonal Rainfall in Western U.S. Summer Streamflow, Geophys. Res. Lett., 50, e2023GL102892, https://doi.org/10.1029/2023gl102892, 2023.

Barnett, T. P., Adam, J. C., and Lettenmaier, D. P.: Potential impacts of a warming climate on water availability in snow-dominated regions, Nature, https://doi.org/10.1038/nature04141, 2005.

Beck, H. E., McVicar, T. R., Vergopolan, N., Berg, A., Lutsko, N. J., Dufour, A., Zeng, Z., Jiang, X., van Dijk, A. I. J. M., and Miralles, D. G.: High-resolution (1 km) Köppen-Geiger maps for 1901–2099 based on constrained CMIP6 projections, Sci. Data, 10, 724, https://doi.org/10.1038/s41597-023-02549-6, 2023.

Bedoya-Maya, F., Shobayo, P., Beckers, J., and van Hassel, E.: The impact of critical water levels on container inland waterway transport, Trans. Res. Pt. D, 131, 104190, https://doi.org/10.1016/j.trd.2024.104190, 2024.

Beria, H., Larsen, J. R., Ceperley, N. C., Michelon, A., Vennemann, T., and Schaefli, B.: Understanding snow hydrological processes through the lens of stable water isotopes, WIREs Water, 5, e1311, https://doi.org/10.1002/wat2.1311, 2018.

Beyers, D. W.: Causal inference in environmental impact studies, J. North Am. Benthol. Soc., 17, 367–373, https://doi.org/10.2307/1468339, 1998.

Biancamaria, S., Cazenave, A., Mognard, N. M., Llovel, W., and Frappart, F.: Satellite-based high latitude snow volume trend, variability and contribution to sea level over 1989/2006, Glob. Planet. Change, 75, 99–107, https://doi.org/10.1016/j.gloplacha.2010.10.011, 2011.

Bolch, T., Kulkarni, A., Kääb, A., Huggel, C., Paul, F., Cogley, J. G., Frey, H., Kargel, J. S., Fujita, K., Scheel, M., Bajracharya, S., and Stoffel, M.: The State and Fate of Himalayan Glaciers, Science, 336, 310–314, https://doi.org/10.1126/science.1215828, 2012.

Breiman, L.: Random Forests, Mach. Learn., 45, 5–32, https://doi.org/10.1023/a:1010933404324, 2001.

Brooks, P. D., Solomon, D. K., Kampf, S., Warix, S., Bern, C., Barnard, D., Barnard, H. R., Carling, G. T., Carroll, R. W. H., Chorover, J., Harpold, A., Lohse, K., Meza, F., McIntosh, J., Neilson, B., Sears, M., and Wolf, M.: Groundwater dominates snowmelt runoff and controls streamflow efficiency in the western United States, Commun. Earth Environ., 6, 341, https://doi.org/10.1038/s43247-025-02303-3, 2025.

Capua, G. D., Runge, J., Donner, R., Hurk, B. v. d., Turner, A., Vellore, R., Krishnan, R., and Coumou, D.: Dominant patterns of interaction between the tropics and mid-latitudes in boreal summer: causal relationships and the role of timescales, Weather Clim. Dynam., https://doi.org/10.5194/wcd-1-519-2020, 2020.

Carlson, G., Massari, C., Rotiroti, M., Bonomi, T., Preziosi, E., Wilder, A., Whitaker, D., and Girotto, M.: Intensive irrigation buffers groundwater declines in key European breadbasket, Nat. Water, 3, 683–692, https://doi.org/10.1038/s44221-025-00445-4, 2025.

Carroll, R. W. H., Niswonger, R. G., Ulrich, C., Varadharajan, C., Siirila-Woodburn, E. R., and Williams, K. H.: Declining groundwater storage expected to amplify mountain streamflow reductions in a warmer world, Nat. Water, 2, 419–433, https://doi.org/10.1038/s44221-024-00239-0, 2024.

Chandel, V. and Ghosh, S.: Components of Himalayan River Flows in a Changing Climate, Water Resour. Res., https://doi.org/10.1029/2020wr027589, 2021.

Chen, X., Parajka, J., Széles, B., Valent, P., Viglione, A., and Blöschl, G.: Impact of Climate and Geology on Event Runoff Characteristics at the Regional Scale, Water, 12, 3457, https://doi.org/10.3390/w12123457, 2020.

Cicuendez, V., Litago, J., Huesca, M., Rodriguez-Rastrero, M., Recuero, L., Merino-de Miguel, S., and Palacios-Orueta, A.: Assessment of the gross primary production dynamics of a Mediterranean holm oak forest by remote sensing time series analysis, Agroforest.Syst., 89, 491–510, https://doi.org/10.1007/s10457-015-9786-x, 2015.

Clarke, G. K. C., Jarosch, A. H., Anslow, F. S., Radic, V., and Menounos, B.: Projected deglaciation of western

Canada in the twenty-first century, Nat. Geosci., 8, 372–377, https://doi.org/10.1038/ngeo2407, 2015.

Coppola, E., Verdecchia, M., Giorgi, F., Colaiuda, V., Tomassetti, B., and Lombardi, A.: Changing hydrological conditions in the Po basin under global warming, Sci. Total Environ., 493, 1183–1196, https://doi.org/10.1016/j.scitotenv.2014.03.003, 2014.

Cowherd, M., Ruby Leung, L., and Girotto, M.: Evolution of global snow drought characteristics from 1850 to 2100, Environ. Res. Lett., 18, 064043, https://doi.org/10.1088/1748-9326/acd804, 2023.

Craig, H.: Isotopic Variations in Meteoric Waters, Science, https://doi.org/10.1126/science.133.3465.1702, 1961.

DeWalle, D. R. and Rango, A.: Principles of Snow Hydrology, Cambridge University Press, ISBN 978-0-521-82362-3, 978-0-511-53567-3, 978-0-521-29032-6, https://doi.org/10.1017/cbo9780511535673, 2008.

Do, H. X., Westra, S., Leonard, M., and Gudmundsson, L.: Global-Scale Prediction of Flood Timing Using Atmospheric Reanalysis, Water Resour. Res., 56, e2019WR024945, https://doi.org/10.1029/2019wr024945, 2020.

Docquier, D., Di Capua, G., Donner, R. V., Pires, C. A. L., Simon, A., and Vannitsem, S.: A comparison of two causal methods in the context of climate analyses, Nonl. Process. Geophys., 31, 115–136, https://doi.org/10.5194/npg-31-115-2024, 2024.

Dorigo, W., Preimesberger, W., Reimer, C., Van der Schalie, R., Pasik, A., De Jeu, R., and Paulik, C.: Soil moisture gridded data from 1978 to present, v202212, ECMVF [data set], https://cds.climate.copernicus.eu/cdsapp#!/dataset/satellite-soil-moisture?tab=overview (last access: 10 November 2025), 2019.

Eckert, N., Corona, C., Giacona, F., Gaume, J., Mayer, S., van Herwijnen, A., Hagenmuller, P., and Stoffel, M.: Climate change impacts on snow avalanche activity and related risks, Nat. Rev. Earth Environ., 5, 369–389, https://doi.org/10.1038/s43017-024-00540-2, 2024.

Fang, B., Bevacqua, E., Rakovec, O., and Zscheischler, J.: An increase in the spatial extent of European floods over the last 70 years, Hydrol. Earth Syst. Sci., 28, 3755–3775, https://doi.org/10.5194/hess-28-3755-2024, 2024.

Food and Agriculture Organization of the United Nations: FAO Land and Water Division, Major hydrological basins of the world, https://data.apps.fao.org/catalog//iso/7707086d-af3c-41cc-8aa5-323d8609b2d1 (last access: 17 July 2025), 2011.

Flynn, H., Fassnacht, S. R., MacDonald, M. S., and Pfohl, A. K. D.: Baseflow from Snow and Rain in Mountain Watersheds, Water, 16, 1665, https://doi.org/10.3390/w16121665, 2024.

Ford, J. D., Pearce, T., Canosa, I. V., and Harper, S.: The rapidly changing Arctic and its societal implications, WIREs Clim. Change, 12, e735, https://doi.org/10.1002/wcc.735, 2021.

Formetta, G., Tootle, G., and Therrell, M.: Regional Reconstruction of Po River Basin (Italy) Streamflow, Hydrology, 9, 163, https://doi.org/10.3390/hydrology9100163, 2022.

François, H., Samacoïts, R., Bird, D. N., Köberl, J., Prettenthaler, F., and Morin, S.: Climate change exacerbates snow-water-energy challenges for European ski tourism, Nat. Clim. Change, 13, 935–942, https://doi.org/10.1038/s41558-023-01759-5, 2023.

Friedl, M., Gray, J., and Sulla-Menashe, D.: MCD12Q2 MODIS-/Terra+Aqua Land Cover Dynamics Yearly L3 Global 500m SIN Grid V006, NASA Land Processes Distributed Active Archive Center, https://doi.org/10.5067/modis/mcd12q2.006, 2019.

Geurts, P., Ernst, D., and Wehenkel, L.: Extremely randomized trees, Mach. Learn., 63, 3–42, https://doi.org/10.1007/s10994-006-6226-1, 2006.

Girotto, M., Reichle, R., Rodell, M., and Maggioni, V.: Data Assimilation of Terrestrial Water Storage Observations to Estimate Precipitation Fluxes: A Synthetic Experiment, Remote Sens., 13, 1223, https://doi.org/10.3390/rs13061223, 2021.

GMAO: Global Modeling and Assimilation Office. MERRA-2 tavg1_2d_lnd_Nx: 2d, 1-Hourly, Time-Averaged, Single-Level, Assimilation, Land Surface Diagnostics V5.12.4 [data set], https://doi.org/10.5067/RKPHT8KC1Y1T, 2015a.

GMAO: Global Modeling and Assimilation Office. MERRA-2 tavg3_2d_glc_Nx: 2d, 3-Hourly, Time-Averaged, Single-Level, Assimilation, Land Ice Surface Diagnostics V5.12.4 [data set], https://doi.org/10.5067/9ETB4TT5J6US, 2015b.

Gordeev, V. V., Pokrovsky, O. S., Zhulidov, A. V., Filippov, A. S., Gurtovaya, T. Y., Holmes, R. M., Kosmenko, L. S., McClelland, J. W., Peterson, B. J., and Tank, S. E.: Dissolved Major and Trace Elements in the Largest Eurasian Arctic Rivers: Ob, Yenisey, Lena, and Kolyma, Water, 16, 316, https://doi.org/10.3390/w16020316, 2024.

Gordon, B. L., Brooks, P. D., Krogh, S. A., Boisrame, G. F. S., Carroll, R. W. H., McNamara, J. P., and Harpold, A. A.: Why does snowmelt-driven streamflow response to warming vary? A data-driven review and predictive framework, Environ. Res. Lett., 17, 053004, https://doi.org/10.1088/1748-9326/ac64b4, 2022.

Gottlieb, A. R. and Mankin, J. S.: Evidence of human influence on Northern Hemisphere snow loss, Nature, 625, 293–300, https://doi.org/10.1038/s41586-023-06794-y, 2024.

Granger, C. W. J.: Investigating Causal Relations by Econometric Models and Cross-spectral Methods, Econometrica, 37, 424–438, https://doi.org/10.2307/1912791, 1969.

Grimaldi, S., Salamon, P., Disperati, J., Zsoter, E., Russo, C., Ramos, A., Carton De Wiart, C., Barnard, C., Hansford, E., Gomes, G., and Prudhomme, C.: River discharge and related historical data from the Global Flood Awareness System, v4.0, Copernicus Emergency Management Service (CEMS) [data set], https://doi.org/10.24381/cds.a4fdd6b9, 2022.

Guastini, E., Zuecco, G., Errico, A., Castelli, G., Bresci, E., Preti, F., and Penna, D.: How does streamflow response vary with spatial scale? Analysis of controls in three nested Alpine catchments, J. Hydrol., 570, 705–718, https://doi.org/10.1016/j.jhydrol.2019.01.022, 2019.

Guo, Y., Yang, Y., Yang, D., Zhang, L., Zheng, H., Xiong, J., Ruan, F., Han, J., and Liu, Z.: Warming leads to both earlier and later snowmelt floods over the past 70 years, Nat. Commun., 16, 3663, https://doi.org/10.1038/s41467-025-58832-0, 2025.

Hall, D. K., Loomis, B. D., DiGirolamo, N. E., and Forman, B. A.: Snowfall Replenishes Groundwater Loss in the Great Basin of the Western United States, but Cannot Compensate for Increasing Aridification, Geophys. Res. Lett., 51, e2023GL107913, https://doi.org/10.1029/2023gl107913, 2024.

Hamed, K. H. and Ramachandra Rao, A.: A modified Mann-Kendall trend test for autocorrelated data, J. Hydrol., 204, 182–196, https://doi.org/10.1016/S0022-1694(97)00125-X, 1998.

Hammond, J. C. and Kampf, S. K.: Subannual Streamflow Responses to Rainfall and Snowmelt Inputs in Snow-Dominated

Watersheds of the Western United States, Water Resour. Res., 56, e2019WR026132, https://doi.org/10.1029/2019wr026132, 2020.

Han, J., Liu, Z., Woods, R., McVicar, T. R., Yang, D., Wang, T., Hou, Y., Guo, Y., Li, C., and Yang, Y.: Streamflow seasonality in a snow-dwindling world, Nature, 629, 1075–1081, https://doi.org/10.1038/s41586-024-07299-y, 2024.

Hasan, M. F., Smith, R., Vajedian, S., Pommerenke, R., and Majumdar, S.: Global land subsidence mapping reveals widespread loss of aquifer storage capacity, Nat. Commun., 14, 6180, https://doi.org/10.1038/s41467-023-41933-z, 2023.

Hasson, S., Böhner, J., and Lucarini, V.: Prevailing climatic trends and runoff response from Hindukush–Karakoram–Himalaya, upper Indus Basin, Earth Syst. Dynam., 8, 337–355, https://doi.org/10.5194/esd-8-337-2017, 2017.

Hersbach, H., Bell, B., Berrisford, P., Biavati, G., Horányi, A., Muñoz Sabater, J., Nicolas, J., Peubey, C., Radu, R., Rozum, I., Schepers, D., Simmons, A., Soci, C., Dee, D., and Thépaut, J.-N.: ERA5 hourly data on single levels from 1940 to present, Copernicus Climate Change Service (C3S) Climate Data Store (CDS) [data set], https://doi.org/10.24381/cds.adbb2d47, 2023.

Huning, L. S. and AghaKouchak, A.: Global snow drought hot spots and characteristics, P. Natl. Acad. Sci. USA, 117, 19753–19759, https://doi.org/10.1073/pnas.1915921117, 2020.

Huss, M.: Present and future contribution of glacier storage change to runoff from macroscale drainage basins in Europe, Water Resour. Res., 47, https://doi.org/10.1029/2010wr010299, 2011.

Huss, M. and Hock, R.: Global-scale hydrological response to future glacier mass loss, Nat. Clim. Change, 8, 135–140, https://doi.org/10.1038/s41558-017-0049-x, 2018.

Immerzeel, W., Beek, L. V. v., and Bierkens, M.: Climate Change Will Affect the Asian Water Towers, Science, https://doi.org/10.1126/science.1183188, 2010.

Immerzeel, W. W., Wanders, N., Lutz, A. F., Shea, J. M., and Bierkens, M. F. P.: Reconciling high-altitude precipitation in the upper Indus basin with glacier mass balances and runoff, Hydrol. Earth Syst. Sci., 19, 4673–4687, https://doi.org/10.5194/hess-19-4673-2015, 2015.

Immerzeel, W. W., Lutz, A. F., Andrade, M., Bahl, A., Biemans, H., Bolch, T., Hyde, S., Brumby, S., Davies, B. J., Elmore, A. C., Emmer, A., Feng, M., Fernández, A., Haritashya, U., Kargel, J. S., Koppes, M., Kraaijenbrink, P. D. A., Kulkarni, A. V., Mayewski, P. A., Nepal, S., Pacheco, P., Painter, T. H., Pellicciotti, F., Rajaram, H., Rupper, S., Sinisalo, A., Shrestha, A. B., Viviroli, D., Wada, Y., Xiao, C., Yao, T., and Baillie, J. E. M.: Importance and vulnerability of the world's water towers, Nature, 577, 364–369, https://doi.org/10.1038/s41586-019-1822-y, 2020.

Inouye, D. W.: Climate change and phenology, WIREs Clim. Change, 13, e764, https://doi.org/10.1002/wcc.764, 2022.

Jiang, S., Bevacqua, E., and Zscheischler, J.: River flooding mechanisms and their changes in Europe revealed by explainable machine learning, Hydrol. Earth Syst. Sci., 26, 6339–6359, https://doi.org/10.5194/hess-26-6339-2022, 2022.

Joshi, S. K., Swarnkar, S., Shukla, S., Kumar, S., Jain, S., and Gautam, S.: Snow/Ice Melt, Precipitation, and Groundwater Contribute to the Sutlej River System, Water Air Soil Pollut., 234, 719, https://doi.org/10.1007/s11270-023-06744-4, 2023.

Julander, R. P. and Clayton, J. A.: Determining the proportion of streamflow that is generated by cold season processes versus summer rainfall in Utah, USA, J. Hydrol. Reg. Stud., 17, 36–46, https://doi.org/10.1016/j.ejrh.2018.04.005, 2018.

Karmouche, S., Galytska, E., Runge, J., Meehl, G. A., Phillips, A. S., Weigel, K., and Eyring, V.: Regime-oriented causal model evaluation of Atlantic–Pacific teleconnections in CMIP6, Earth Syst. Dynam., 14, 309–344, https://doi.org/10.5194/esd-14-309-2023, 2023.

Kashyap, A. and Behera, M. D.: Excess topography and outburst flood: Geomorphic imprint of October 2023 extreme flood event in the Teesta catchment of Eastern Himalayas, Glob. Planet. Change, 240, 104540, https://doi.org/10.1016/j.gloplacha.2024.104540, 2024.

Kathpalia, A., Manshour, P., and Paluš, M.: Compression complexity with ordinal patterns for robust causal inference in irregularly sampled time series, Sci. Rep., 12, 14170, https://doi.org/10.1038/s41598-022-18288-4, 2022.

Kim, H., Fastovich, D., Bhattacharya, T., and Tuttle, S.: Improving predictions of snow resources using midlatitude SSTs with convergent cross mapping, Environ. Res. Clim., 4, 021001, https://doi.org/10.1088/2752-5295/add362, 2025.

Kolluru, V., John, R., Chen, J., Konkathi, P., Kolluru, S., Saraf, S., Henebry, G. M., Xiao, J., Jain, K., and Kussainova, M.: Dominant role of grazing and snow cover variability on vegetation shifts in the drylands of Kazakhstan, Commun. Earth Environ., 5, 424, https://doi.org/10.1038/s43247-024-01587-1, 2024.

Koya, S. R., Kar, K. K., and Roy, T.: Northern Pacific sea-level pressure controls rain-on-snow in North America, Commun. Earth Environ., 5, 260, https://doi.org/10.1038/s43247-024-01431-6, 2024.

Kretschmer, M., Coumou, D., Donges, J. F., and Runge, J.: Using Causal Effect Networks to Analyze Different Arctic Drivers of Midlatitude Winter Circulation, J. Clim., 29, 4069–4081, https://doi.org/10.1175/jcli-d-15-0654.1, 2016.

Krogh, S. A. and Pomeroy, J. W.: Recent changes to the hydrological cycle of an Arctic basin at the tundra–taiga transition, Hydrol. Earth Syst. Sci., 22, 3993–4014, https://doi.org/10.5194/hess-22-3993-2018, 2018.

Kumar, N., Ganguly, A., Biswal, K., Keesari, T., Pandey, A., and Deshpande, R.: Relative contribution from different water sources to supraglacial runoff in western Himalaya, J. Hydrol., 635, 131137, https://doi.org/10.1016/j.jhydrol.2024.131137, 2024.

Kumar, S. V., Jasinski, M., Mocko, D. M., Rodell, M., Borak, J., Li, B., Beaudoing, H. K., and Peters-Lidard, C. D.: NCA-LDAS Land Analysis: Development and Performance of a Multisensor, Multivariate Land Data Assimilation System for the National Climate Assessment, J. Hydrometeorol., 20, 1571–1593, https://doi.org/10.1175/jhm-d-17-0125.1, 2019.

Kurylyk, B. L. and Walvoord, M. A.: Permafrost Hydrogeology, in: Arctic Hydrology, Permafrost and Ecosystems, edited by: Yang, D. and Kane, D. L., Springer, Cham, https://doi.org/10.1007/978-3-030-50930-9_17, 2021.

Lambrecht, A. and Mayer, C.: The role of the cryosphere for runoff in a highly glacierised alpine catchment, an approach with a coupled model and in situ data, J. Glaciol., 70, e33, https://doi.org/10.1017/jog.2024.48, 2024.

Li, D., Wrzesien, M. L., Durand, M., Adam, J., and Lettenmaier, D. P.: How much runoff originates as snow in the western United States, and how will that change in the future?, Geophys. Res.

Lett., 44, 6163–6172, https://doi.org/10.1002/2017gl073551, 2017.

Li, D., Lettenmaier, D. P., Margulis, S. A., and Andreadis, K.: The Role of Rain-on-Snow in Flooding Over the Conterminous United States, Water Resour. Res., 55, 8492–8513, https://doi.org/10.1029/2019wr024950, 2019.

Li, S., Wang, G., Zhu, C., Hannemann, M., Poyatos, R., Lu, J., Li, J., Ullah, W., Hagan, D. F. T., García-García, A., Liu, Y., Liu, Q., Ma, S., Liu, Q., Sun, S., Zhao, F., and Peng, J.: Spatial patterns and recent temporal trends in global transpiration modelled using eco-evolutionary optimality, Agr. Forest Meteorol., 342, 109702, https://doi.org/10.1016/j.agrformet.2023.109702, 2023.

Liang, X. S. and Kleeman, R.: Information Transfer between Dynamical System Components, Phys. Rev. Lett., 95, 244101, https://doi.org/10.1103/PhysRevLett.95.244101, 2005.

Lucianetti, G., Penna, D., Mastrorillo, L., and Mazza, R.: The Role of Snowmelt on the Spatio-Temporal Variability of Spring Recharge in a Dolomitic Mountain Group, Italian Alps, Water, https://doi.org/10.3390/w12082256, 2020.

Lutz, A. F., Immerzeel, W. W., Shrestha, A. B., and Bierkens, M. F. P.: Consistent increase in High Asia's runoff due to increasing glacier melt and precipitation, Nat. Clim. Change, https://doi.org/10.1038/nclimate2237, 2014.

López-Moreno, J., Granados, I., Ceballos-Barbancho, A., Morán-Tejeda, E., Revuelto, J., Alonso-González, E., Gascoin, S., Herrero, J., Deschamps-Berger, C., and Latron, J.: The signal of snowmelt in streamflow and stable water isotopes in a high mountain catchment in Central Spain, J. Hydrol. Reg. Stud., https://doi.org/10.1016/j.ejrh.2023.101356, 2023.

Maina, F. Z. and Kumar, S. V.: Diverging Trends in Rain-On-Snow Over High Mountain Asia, Earth's Future, 11, e2022EF003009, https://doi.org/10.1029/2022ef003009, 2023.

Mavromatis, V., Rinder, T., Prokushkin, A. S., Pokrovsky, O. S., Korets, M. A., Chmeleff, J., and Oelkers, E. H.: The effect of permafrost, vegetation, and lithology on Mg and Si isotope composition of the Yenisey River and its tributaries at the end of the spring flood, Geochim. Cosmochim. Ac., 191, 32–46, https://doi.org/10.1016/j.gca.2016.07.003, 2016.

Miralles, D. G., Bonte, O., Koppa, A., Baez-Villanueva, O. M., Tronquo, E., Zhong, F., Beck, H. E., Hulsman, P., Dorigo, W., Verhoest, N. E. C., and Haghdoost, S.: GLEAM4: global land evaporation and soil moisture dataset at 0.1° resolution from 1980 to near present, Sci. Data, 12, 416, https://doi.org/10.1038/s41597-025-04610-y, 2025.

Mohseni, F., Jamali, S., Ghorbanian, A., and Mokhtarzade, M.: Global soil moisture trend analysis using microwave remote sensing data and an automated polynomial-based algorithm, Glob. Planet. Change, 231, 104310, https://doi.org/10.1016/j.gloplacha.2023.104310, 2023.

Mudryk, L., Mortimer, C., Derksen, C., Elias Chereque, A., and Kushner, P.: Benchmarking of snow water equivalent (SWE) products based on outcomes of the SnowPEx+ Intercomparison Project, The Cryosphere, 19, 201–218, https://doi.org/10.5194/tc-19-201-2025, 2025.

Musselman, K. N., Clark, M. P., Liu, C., Ikeda, K., and Rasmussen, R.: Slower snowmelt in a warmer world, Nat. Clim. Change, 7, 214–219, https://doi.org/10.1038/nclimate3225, 2017.

Musselman, K. N., Lehner, F., Ikeda, K., Clark, M. P., Prein, A. F., Liu, C., Barlage, M., and Rasmussen, R.: Projected increases and shifts in rain-on-snow flood risk over western North America, Nat. Clim. Change, https://doi.org/10.1038/s41558-018-0236-4, 2018.

Muñoz Sabater, J.: ERA5-Land hourly data from 1950 to present, Copernicus Climate Change Service (C3S) Climate Data Store (CDS) [data set], https://doi.org/10.24381/cds.e2161bac, 2019.

Norton, C. L., Dannenberg, M. P., Yan, D., Wallace, C. S. A., Rodriguez, J. R., Munson, S. M., van Leeuwen, W. J. D., and Smith, W. K.: Climate and Socioeconomic Factors Drive Irrigated Agriculture Dynamics in the Lower Colorado River Basin, Remote Sens., 13, 1659, https://doi.org/10.3390/rs13091659, 2021.

Park, H., Kim, Y., Suzuki, K., and Hiyama, T.: Influence of snowmelt on increasing Arctic river discharge: numerical evaluation, Prog. Earth Planet. Sci., 11, 13, https://doi.org/10.1186/s40645-024-00617-y, 2024.

Pearl, J.: CAUSALITY: MODELS, REASONING, AND INFERENCE, Cambridge University Press, ISBN 13: 9780521773621, 2000.

Penna, D., Engel, M., Bertoldi, G., and Comiti, F.: Towards a tracer-based conceptualization of meltwater dynamics and streamflow response in a glacierized catchment, Hydrol. Earth Syst. Sci., 21, 23–41, https://doi.org/10.5194/hess-21-23-2017, 2017.

Philippon, N., Mougin, E., Jarlan, L., and Frison, P. L.: Analysis of the linkages between rainfall and land surface conditions in the West African monsoon through CMAP, ERS-WSC, and NOAA-AVHRR data, J. Geophys. Res.-Atmos., 110, D24115, https://doi.org/10.1029/2005jd006394, 2005.

Pritchard, H. D.: Asia's shrinking glaciers protect large populations from drought stress, Nature, 569, 649–654, https://doi.org/10.1038/s41586-019-1240-1, 2019.

Pulliainen, J., Luojus, K., Derksen, C., Mudryk, L., Lemmetyinen, J., Salminen, M., Ikonen, J., Takala, M., Cohen, J., Smolander, T., and Norberg, J.: Patterns and trends of Northern Hemisphere snow mass from 1980 to 2018, Nature, https://doi.org/10.1038/s41586-020-2258-0, 2020.

Pérez Valentín, J. M. and Müller, M. F.: Impact of Hurricane Maria on Beach Erosion in Puerto Rico: Remote Sensing and Causal Inference, Geophys. Res. Lett., 47, e2020GL087306, https://doi.org/10.1029/2020gl087306, 2020.

Qin, Y., Hong, C., Zhao, H., Siebert, S., Abatzoglou, J. T., Huning, L. S., Sloat, L. L., Park, S., Li, S., Munroe, D. K., Zhu, T., Davis, S. J., and Mueller, N. D.: Snowmelt risk telecouplings for irrigated agriculture, Nat. Clim. Change, 12, 1007–1015, https://doi.org/10.1038/s41558-022-01509-z, 2022.

Rawlins, M. A., Fahnestock, M., Frolking, S., and Vörösmarty, C. J.: On the evaluation of snow water equivalent estimates over the terrestrial Arctic drainage basin, Hydrol. Proc., 21, 1616–1623, https://doi.org/10.1002/hyp.6724, 2007.

Reyes-García, V., García-Del-Amo, D., Porcuna-Ferrer, A., Schlingmann, A., Abazeri, M., Attoh, E. M. N. A. N., Vieira da Cunha Ávila, J., Ayanlade, A., Babai, D., Benyei, P., Calvet-Mir, L., Carmona, R., Caviedes, J., Chah, J., Chakauya, R., Cuní-Sanchez, A., Fernández-Llamazares, A., Galappaththi, E. K., Gerkey, D., Graham, S., Guillerminet, T., Huanca, T., Ibarra, J. T., Junqueira, A. B., Li, X., López-Maldonado, Y., Mattalia, G., Samakov, A., Schunko, C., Seidler, R., Sharakhmatova, V., Singh, P., Tofighi-Niaki, A., Torrents-Ticó, M., Álvarez Fernández, S., Bulamah, R. C., Chambon, M., Chao, O., Chen, Z., Chengula, F., Cruz-Gispert, A., Demichelis, C., Dudina, E., Gallois,

S., Glauser, M., Guillerminet, T., Hirsch, E., Izquierdo, A. E., Junsberg, L., Mariel, J., Miara, M. D., Miñarro, S., Porcher, V., Shrestha, U. B., Sharma, A., Ulambayar, T., Wu, R., Zakari, I. S., Zant, M., and LICCI Consortium: Local studies provide a global perspective of the impacts of climate change on Indigenous Peoples and local communities, Sustain. Earth Rev., 7, 1, https://doi.org/10.1186/s42055-023-00063-6, 2024.

RGI 7.0 Consortium: Randolph Glacier Inventory – A Dataset of Global Glacier Outlines, Version 7.0, https://doi.org/10.5067/f6jmovy5navz, 2023.

Robinson, E. L. and Clark, D. B.: Using Gravity Recovery and Climate Experiment data to derive corrections to precipitation data sets and improve modelled snow mass at high latitudes, Hydrol. Earth Syst. Sci., 24, 1763–1779, https://doi.org/10.5194/hess-24-1763-2020, 2020.

Runge, J.: Conditional independence testing based on a nearest-neighbor estimator of conditional mutual information, in: Proceedings of the Twenty-First International Conference on Artificial Intelligence and Statistics, 938–947, PMLR, https://proceedings.mlr.press/v84/runge18a.html (last access: 16 June 2026), 2018.

Runge, J.: Discovering contemporaneous and lagged causal relations in autocorrelated nonlinear time series datasets, in: Proceedings of the 36th Conference on Uncertainty in Artificial Intelligence (UAI), edited by: Peters, J. and Sontag, D., Vol. 124, Proceedings of Machine Learning Research,1388–1397, PMLR, https://proceedings.mlr.press/v124/runge20a.html (last access: 16 June 2026), 2020.

Runge, J.: Necessary and sufficient graphical conditions for optimal adjustment sets in causal graphical models with hidden variables, in: Advances in Neural Information Processing Systems, Vol. 34, 15762–15773, Curran Associates, Inc., https://proceedings.neurips.cc/paper/2021/hash/8485ae387a981d783f8764e508151cd9-Abstract.html (last access: 16 June 2026), 2021.

Runge, J., Heitzig, J., Marwan, N., and Kurths, J.: Quantifying Causal Coupling Strength: A Lag-specific Measure For Multivariate Time Series Related To Transfer Entropy, Arxiv, https://doi.org/10.48550/arxiv.1210.2748, 2012.

Runge, J., Nowack, P., Kretschmer, M., Flaxman, S., and Sejdinovic, D.: Detecting and quantifying causal associations in large nonlinear time series datasets, Sci. Adv., 5, eaau4996, https://doi.org/10.1126/sciadv.aau4996, 2019.

Runge, J., Gerhardus, A., Varando, G., Eyring, V., and Camps-Valls, G.: Causal inference for time series, Nat. Rev. Earth Environ., 4, 487–505, https://doi.org/10.1038/s43017-023-00431-y, 2023.

Schilling, S., Dietz, A., and Kuenzer, C.: Snow Water Equivalent Monitoring – A Review of Large-Scale Remote Sensing Applications, Remote Sens., 16, 1085, https://doi.org/10.3390/rs16061085, 2024.

Schweighofer, J.: The impact of extreme weather and climate change on inland waterway transport, Nat. Hazard., 72, 23–40, https://doi.org/10.1007/s11069-012-0541-6, 2014.

Sen, P. K.: Estimates of the Regression Coefficient Based on Kendall's Tau, J. Am. Stat. Assoc., 63, 1379–1389, https://doi.org/10.1080/01621459.1968.10480934, 1968.

Shafeeque, M., Luo, Y., Arshad, A., Muhammad, S., Ashraf, M., and Pham, Q. B.: Assessment of climate change impacts on glacio-hydrological processes and their variations within critical zone, Nat. Hazard., 115, 2721–2748, https://doi.org/10.1007/s11069-022-05661-9, 2023.

Sharif, M., Archer, D. R., Fowler, H. J., and Forsythe, N.: Trends in timing and magnitude of flow in the Upper Indus Basin, Hydrol. Earth Syst. Sci., 17, 1503–1516, https://doi.org/10.5194/hess-17-1503-2013, 2013.

Shi, X., Qin, T., Nie, H., Weng, B., and He, S.: Changes in Major Global River Discharges Directed into the Ocean, Int. J. Environ. Res. Public Hea., 16, 1469, https://doi.org/10.3390/ijerph16081469, 2019.

Slater, L. and Binley, A.: Advancing hydrological process understanding from long-term resistivity monitoring systems, WIREs Water, 8, e1513, https://doi.org/10.1002/wat2.1513, 2021.

Slatyer, R. A., Umbers, K. D. L., and Arnold, P. A.: Ecological responses to variation in seasonal snow cover, Conserv. Biol., 36, e13727, https://doi.org/10.1111/cobi.13727, 2024.

Snethlage, M., Geschke, J., Spehn, E., Ranipeta, A., Yoccoz, N., Körner, C., Jetz, W., Fischer, M., and Urbach, D.: GMBA Mountain Inventory v2, GMBA-EarthEnv, https://doi.org/10.48601/earthenv-t9k2-1407, 2022.

Sogno, P., Klein, I., Uereyen, S., Bachofer, F., and Kuenzer, C.: Surface water dynamics of Africa: Analysing continental trends and identifying drivers for major lakes and reservoirs, Int. J. Remote Sens., 45, 9538–9568, https://doi.org/10.1080/01431161.2024.2412802, 2024.

Soheb, M., Bastian, P., Schmidt, S., Singh, S., Kaushik, H., Ramanathan, A., and Nüsser, M.: Surface and subsurface flow of a glacierised catchment in the cold-arid region of Ladakh, Trans-Himalaya, J. Hydrol., 635, 131063, https://doi.org/10.1016/j.jhydrol.2024.131063, 2024.

Soomro, S.-e.-h., Soomro, A. R., Batool, S., Guo, J., Li, Y., Bai, Y., Hu, C., Tayyab, M., Zeng, Z., Li, A., Zhen, Y., Rui, K., Hameed, A., and Wang, Y.: How does the climate change effect on hydropower potential, freshwater fisheries, and hydrological response of snow on water availability?, Appl. Water Sci., 14, 65, https://doi.org/10.1007/s13201-023-02070-6, 2024.

Spirtes, P.: Discovering causal relations among latent variables in directed acyclic graphical models, Tech. rep., Carnegie Mellon, Pittsburgh, https://www.cmu.edu/dietrich/philosophy/docs/tech-reports/69_Spirtes.pdf (last access: 16 June 2026), 1996.

Stagl, J. C. and Hattermann, F. F.: Impacts of Climate Change on the Hydrological Regime of the Danube River and Its Tributaries Using an Ensemble of Climate Scenarios, Water, 7, 6139–6172, https://doi.org/10.3390/w7116139, 2015.

Sun, A. Y., Save, H., Rateb, A., Jiang, P., and Scanlon, B. R.: Deciphering the Role of Total Water Storage Anomalies in Mediating Regional Flooding, Geophys. Res. Lett., 51, e2023GL108126, https://doi.org/10.1029/2023gl108126, 2024.

Sun, Q., Zhang, X., Zwiers, F., Westra, S., and Alexander, L. V.: A Global, Continental, and Regional Analysis of Changes in Extreme Precipitation, J. Clim., 34, 243–258, https://doi.org/10.1175/jcli-d-19-0892.1, 2021.

Tague, C. and Grant, G. E.: Groundwater dynamics mediate low-flow response to global warming in snow-dominated alpine regions, Water Resour. Res., 45, https://doi.org/10.1029/2008wr007179, 2009.

Talsma, C. J., Bennett, K. E., and Vesselinov, V. V.: Characterizing Drought Behavior in the Colorado River Basin Using Unsuper-

vised Machine Learning, Earth Space Sci., 9, e2021EA002086, https://doi.org/10.1029/2021ea002086, 2022.

Tangdamrongsub, N., Hwang, C., Borak, J. S., Prabnakorn, S., and Han, J.: Optimizing GRACE/GRACE-FO data and a priori hydrological knowledge for improved global terrestrial water storage component estimates, J. Hydrol., 598, 126463, https://doi.org/10.1016/j.jhydrol.2021.126463, 2021.

Tong, J., Déry, S. J., Jackson, P. L., and Derksen, C.: Snow distribution from SSM/I and its relationships to the hydroclimatology of the Mackenzie River Basin, Canada, Adv. Water Resour., 33, 667–677, https://doi.org/10.1016/j.advwatres.2010.03.009, 2010.

Uereyen, S., Bachofer, F., and Kuenzer, C.: A Framework for Multivariate Analysis of Land Surface Dynamics and Driving Variables – A Case Study for Indo-Gangetic River Basins, Remote Sens., 14, 197, https://doi.org/10.3390/rs14010197, 2022.

Ultee, L., Coats, S., and Mackay, J.: Glacial runoff buffers droughts through the 21st century, Earth Syst. Dynam., 13, 935–959, https://doi.org/10.5194/esd-13-935-2022, 2022.

UN DESA: United Nations Department of Economic and Social Affairs, World Population Prospects 2022: Summary of Results, Tech. Rep. 3, United Nations Department of Economic and Social Affairs, https://www.un.org/development/desa/pd/sites/www.un.org.development.desa.pd/files/wpp2022_summary_of_results.pdf (last access: 15 September 2025), 2022.

Van Tiel, M., Van Loon, A. F., Seibert, J., and Stahl, K.: Hydrological response to warm and dry weather: do glaciers compensate?, Hydrol. Earth Syst. Sci., 25, 3245–3265, https://doi.org/10.5194/hess-25-3245-2021, 2021.

Vezzoli, R., Mercogliano, P., Pecora, S., Zollo, A. L., and Cacciamani, C.: Hydrological simulation of Po River (North Italy) discharge under climate change scenarios using the RCM COSMO-CLM, Sci. Total Environ., 521/522, 346–358, https://doi.org/10.1016/j.scitotenv.2015.03.096, 2015.

Viviroli, D., Dürr, H. H., Messerli, B., Meybeck, M., and Weingartner, R.: Mountains of the world, water towers for humanity: Typology, mapping, and global significance, Water Resour. Res., 43, https://doi.org/10.1029/2006wr005653, 2007.

Vyshnevskyi, V. and Shevchuk, S.: Impact of climate change and human factors on the water regime of the Danube Delta, Acta Hydrol. Slov., 23, 207–216, https://doi.org/10.31577/ahs-2022-0023.02.0023, 2022.

Wang, H., Liu, J., Klaar, M., Chen, A., Gudmundsson, L., and Holden, J.: Anthropogenic climate change has influenced global river flow seasonality, Science, 383, 1009–1014, https://doi.org/10.1126/science.adi9501, 2024.

Wang, P., Huang, Q., Pozdniakov, S. P., Liu, S., Ma, N., Wang, T., Zhang, Y., Yu, J., Xie, J., Fu, G., Frolova, N. L., and Liu, C.: Potential role of permafrost thaw on increasing Siberian river discharge, Environ. Res. Lett., 16, 034046, https://doi.org/10.1088/1748-9326/abe326, 2021.

Wang, S., Zhou, F., and Russell, H.: Estimating Snow Mass and Peak River Flows for the Mackenzie River Basin Using GRACE Satellite Observations, Remote Sens., 9, 256, https://doi.org/10.3390/rs9030256, 2017.

Wang, Y., Shen, Y., and Zhang, X.: Shifts in snowmelt runoff timing and their driving factors in the Upper Indus Basin, Chinese Journal of Eco-Agriculture, 34, 1070–1083, https://doi.org/10.12357/cjea.20250451, 2026.

Wang, Y.-R., Hessen, D. O., Samset, B. H., and Stordal, F.: Evaluating global and regional land warming trends in the past decades with both MODIS and ERA5-Land land surface temperature data, Remote Sens. Environ., 280, 113181, https://doi.org/10.1016/j.rse.2022.113181, 2022.

Webb, R. W., Knowles, J. F., Fox, A., Fabricus, A., Corrie, T., Mooney, K., Gallais, J., Frimpong, N. A. G., Akurugu, C. A., Barron-Gafford, G., Blanken, P. D., Burns, S. P., Frank, J., and Litvak, M.: Energy-Water Asynchrony Principally Determines Water Available for Runoff From Snowmelt in Continental Montane Forests, Hydrol. Proc., 38, e15297, https://doi.org/10.1002/hyp.15297, 2024.

Wenzl, M., Baumhoer, C. A., Dietz, A. J., and Kuenzer, C.: Vegetation Changes in the Arctic: A Review of Earth Observation Applications, Remote Sens., 16, 4509, https://doi.org/10.3390/rs16234509, 2024.

Wolf, M. A., Jamison, L. R., Solomon, D. K., Strong, C., and Brooks, P. D.: Multi-Year Controls on Groundwater Storage in Seasonally Snow-Covered Headwater Catchments, Water Resour. Res., 59, e2022WR033394, https://doi.org/10.1029/2022wr033394, 2023.

Woo, M.-k., Thorne, R., and Brown, L.: Comparison of runoff and river flow in two large northern basins, Hydrol. Res., 50, 1609–1622, https://doi.org/10.2166/nh.2018.199, 2018.

Wu, X., Zhu, R., Long, Y., and Zhang, W.: Spatial Trend and Impact of Snowmelt Rate in Spring across China's Three Main Stable Snow Cover Regions over the Past 40 Years Based on Remote Sensing, Remote Sens., 14, 4176, https://doi.org/10.3390/rs14174176, 2022.

Xu, C., Chen, Y., Hamid, Y., Tashpolat, T., Chen, Y., Ge, H., and Li, W.: Long-term change of seasonal snow cover and its effects on river runoff in the Tarim River basin, northwestern China, Hydrol. Proc., 23, 2045–2055, https://doi.org/10.1002/hyp.7334, 2009.

Yang, D., Shrestha, R. R., Lung, J. L. Y., Tank, S., and Park, H.: Heat flux, water temperature and discharge from 15 northern Canadian rivers draining to Arctic Ocean and Hudson Bay, Glob. Planet. Change, 204, 103577, https://doi.org/10.1016/j.gloplacha.2021.103577, 2021.

Yao, T., Bolch, T., Chen, D., Gao, J., Immerzeel, W., Piao, S., Su, F., Thompson, L., Wada, Y., Wang, L., Wang, T., Wu, G., Xu, B., Yang, W., Zhang, G., and Zhao, P.: The imbalance of the Asian water tower, Nat. Rev. Earth Environ., 3, 618–632, https://doi.org/10.1038/s43017-022-00299-4, 2022.

Yuan, S., Liu, Y., Liu, Y., Zhang, K., Li, Y., Enwer, R., Li, Y., and Hu, Q.: Spatiotemporal variations of surface albedo in Central Asia and its influencing factors and confirmatory path analysis during the 21st century, Int. J. Appl. Earth Observ. Geo., 134, 104233, https://doi.org/10.1016/j.jag.2024.104233, 2024.

Zakharova, E. A., Kouraev, A. V., Biancamaria, S., Kolmakova, M. V., Mognard, N. M., Zemtsov, V. A., Kirpotin, S. N., and Decharme, B.: Snow Cover and Spring Flood Flow in the Northern Part of Western Siberia (the Poluy, Nadym, Pur, and Taz Rivers), J. Hydrometeorol., 12, 1498–1511, https://doi.org/10.1175/jhm-d-11-017.1, 2011.

Zhang, Y., He, B., Guo, L., and Liu, D.: Differences in Response of Terrestrial Water Storage Components to Precipitation over 168 Global River Basins, J. Hydrometeorol., 20, 1981–1999, https://doi.org/10.1175/jhm-d-18-0253.1, 2019.

Zhang, Z., Wang, D., Wu, X., Mei, Y., Qiu, J., and Zhu, J.: Unveiling flood-generating mechanisms using circular statistics-based machine learning approach without the need for discharge data during inference, Hydrol. Res., 54, https://doi.org/10.2166/nh.2023.058, 2023.

Zhou, H., Zhang, L., Liu, X., Liang, D., Zhu, Q., and Gou, Y.: Study of the Relationship between High Mountain Asia Snow Cover and Drought and Flood in the Yangtze River Basin during 1980–2019, Remote Sens., https://doi.org/10.3390/rs14153588, 2022.

Zhu, L. and Meng, J.: Determining the relative importance of climatic drivers on spring phenology in grassland ecosystems of semi-arid areas, Int. J. Biometeorol., 59, 237–248, https://doi.org/10.1007/s00484-014-0839-z, 2015.